NASA/TP—2001–209991

Modeling Biogeochemical-Physical Interactions and Carbon Flux in the Sargasso Sea (Bermuda Atlantic Time-series Study site)

Sergio R. Signorini, SAIC, Beltsville, Maryland
Charles R. McClain, Office for Global Carbon Studies, NASA Goddard Space Flight Center, Greenbelt, Maryland
James R. Christian, University of Maryland, ESSIC, College Park, Maryland

National Aeronautics and
Space Administration

Goddard Space Flight Center
Greenbelt, Maryland 20771

October 2001

Acknowledgments

This work was supported by the NASA Ocean Biogeochemistry Program. We are very thankful to Dave Siegel (Institute for Computational Earth System Science, UCSB) and Rod Johnson (Bermuda Biological Station for Research, Inc.) for facilitating the access to the BATS and BBOP data sets. We also acknowledge the technicians, R.V. Weatherbird II crew, and BATS PI's for providing high-quality data sets and invaluable scientific contributions.

Available from:

NASA Center for AeroSpace Information
7121 Standard Drive
Hanover, MD 21076-1320
Price Code: A17

National Technical Information Service
5285 Port Royal Road
Springfield, VA 22161
Price Code: A10

PROLOGUE

A one dimensional, coupled ecosystem/carbon cycle model is used to analyze the biogeochemical-physical interactions and carbon fluxes in the Bermuda Atlantic Time-series Study (BATS) site for the period of 1992-1998. The influence of mesoscale eddies (remote forcing) is taken into account via nutricline displacements and vertical advection derived from satellite altimetry. Physical forcing and biogeochemical boundary conditions are derived from the comprehensive BATS data sets. The observed parameters not used for model forcing and boundary conditions are used to verify model performance. The model results compare well with observations (most variables are within 8% of observed values). The new production predicted by the model, 0.47±0.14 mol N m^{-2} yr^{-1}, is within 6% of the 0.50±0.15 mol N m^{-2} yr^{-1} mean estimate for the Sargasso Sea reported by *Siegel et al.* [1999]. The mean (1992-1998) sea-air CO_2 flux was -0.3 mol C m^{-2} yr^{-1}, indicating that the BATS region is a weak sink of atmospheric CO_2. This estimate was obtained with the *Wanninkhof* [1992] gas transfer algorithm, which provides a ΔpCO_2 range within 2.5% of the observed value. However, the sea-air flux varies depending upon the gas transfer algorithm used. Four of the five algorithms used provide a reasonable (≤10%) match with the observed ΔpCO_2. The sea-air flux obtained with the use of these algorithms ranges from -0.32 to -0.50 mol C m^{-2} yr^{-1}, which is within the range (-0.22 to -0.83 mol C m^{-2} yr^{-1}) of previously reported values [*Bates et al.*, 1996; *Bates et al.*, 1998d]. The model reveals prominent seasonal TCO_2 variability, primarily due to SST and total alkalinity (TA) changes. The seasonal variability of surface layer TA is quite large. For the period of model simulation (1992-1998), the TA ranged between a low of 2364 μmol kg^{-1} and a high of 2404 μmol kg^{-1}. A significant portion of the TA variability is due to salinity changes via the effects of evaporation and precipitation [*Bates et al.*, 1996]. The minimum TA (2364 μmol kg^{-1}) occurred on August 1998, during the peak of La Niña in the tropical Pacific. This minimum TA occurred during the period's warmest SST (28.4°C), lowest surface salinity (36.23), highest pCO_2 (420 μatm), and lowest TCO_2 (2018 μmol kg^{-1}). The overall carbon balance (fluxes through the surface and bottom boundary at 350 meters) consists atmospheric CO_2 uptake of 0.3 mol C m^{-2} yr^{-1}, upward DIC bottom flux via mixing and advection of 1.1 mol C m^{-2} yr^{-1}, and carbon export of 1.4 mol C m^{-2} yr^{-1} via sedimentation. Upper ocean TCO_2 levels increased between 1992 and 1996 at a rate of ~1.2 μmol kg^{-1} yr^{-1}, consistent with observations [*Bates et al.*, 1996; *Bates*, 2001]. However, this trend was reversed during 1997-1998 to –2.7 μmol kg^{-1} yr^{-1}. This large change in TCO_2 trend coincided with a significant TA drop (~9 μmol kg^{-1}) from 1997 to 1998, in response to hydrographic changes imposed by the El Niño-La Niña transition, which were manifested in the Sargasso Sea by the warmest SST and lowest surface salinity of the period (1992-1998).

1. Introduction

Bermuda is the site of some of the longest-running ocean and atmosphere time-series investigations. The linchpin of oceanographic time-series in Bermuda is the Hydrostation S program, started by Henry Stommel (Woods Hole Oceanographic Institution) and co-workers in 1954. Hydrostation S is located ~22 km southeast of Bermuda (32° 10'N, 64° 30'W). The comprehensive long-term physical and biogeochemical data originating from Hydrostation S are invaluable for interpreting the interannual patterns in the physical structure of the ocean [e.g., *Schroeder et al.*, 1959; *Schroeder and Stommel*, 1969; *Pocklington*, 1972; *Wunsch*, 1972], the seasonal cycle of nutrients, chlorophyll, and primary production in the Sargasso Sea [e.g., *Menzel and Ryther*, 1960; *Menzel and Ryther* ,1961], and ocean biogeochemistry in general.

In October 1988 the Bermuda Atlantic Time-series Study (BATS) commenced sampling the Sargasso Sea in an area 85 km southeast of Bermuda (31°45'N, 64°10'W) as part of the U.S. Joint Global Ocean Flux Study (JGOFS). The scientific goal of the BATS program is to understand the causes of seasonal and interannual variability in ocean biogeochemistry, both at the BATS study site and as it may relate to biogeochemistry of the rest of the ocean [*Michaels and Knap*, 1996].

The biogeochemistry near Bermuda is influenced by strong seasonal meridional gradients. There is weak mixing to the south of Bermuda which leads to a permanently stratified water column of oligotrophic characteristics throughout the year [*Michaels and Knap*, 1996]. Nitrate is rarely present at the surface, the ecosystem is dominated by picoplankton and the microbial food web, and nitrogen-fixing cyanobacteria are common [*Carpenter*, 1983; *Olson et al.*, 1990a,b; *Siegel et al.*, 1990]. In contrast, the deep winter mixed layers to the north of Bermuda result in blooms of larger phytoplankton, including diatoms and coccolithophores, and a complex transition to oligotrophy in the summer [*Siegel et al.*, 1990]. Both of these seasonal patterns can occur at the BATS site depending on the intensity of winter mixing [*Michaels and Knap*, 1996].

Many unanswered questions remain regarding the nutrient and carbon balances at BATS. Previous efforts to achieve closure on the carbon budget at BATS [*Michaels et al.*, 1994b] revealed a large residual discrepancy (~8 mmol C m^{-2} d^{-1}). The uncertainties in the vertical fluxes were very small except for two processes, particle settling and horizontal advection. A first-order carbon balance required either that the shallow sediment traps under-collected sinking particles by as much as a factor of 5 or that up to 70% of the carbon dynamics are determined by advection, or some combination of both [*Michaels et al.*, 1994b].

In this study, we combine existing long-term data sets with the use of a one-dimensional ecosystem model to investigate the physical and biogeochemical processes that govern the carbon and nutrient cycles at BATS. Considering the limitations of the one-dimensional dynamics, the influence of mesoscale eddies (remote forcing) is taken into account via nutricline displacements and vertical advection derived from satellite altimetry. The outstanding question of how influential horizontal advection is to the seasonal fluxes of nutrients and carbon will remain unanswerable until three-dimensional field studies are conducted at BATS. However, our study shows that a large uncertainty remains in the determination of the air-sea CO_2 flux depending on the formulation used. One of the main objectives of this study is to evaluate the effects of the different gas exchange formulations on the carbon balance in the Sargasso Sea. In addition, the model provides an extension for the seasonal and interannual analysis beyond the available observations. This is more evident for the ΔpCO_2 record, for which only 2.5 years of observations are currently available (1994-1996).

2. Data Sources

The ecosystem model is physically forced by temperature, salinity, and mixed layer depth derived from BATS data. The data sets from BATS are discussed in several previous studies [*Bates et al.*, 1996; *Michaels et al.*, 1994a; *Michaels and Knap*, 1996]. The BATS biogeochemical data were used for model validation. The mixed layer and PAR time series were obtained from the Bermuda Bio-Optics Program (BBOP) data base. The mixed layer depth (D_{mld}) was calculated by finding the first depth where $\sigma_\theta(D_{mld}) - \sigma_\theta(0) = \alpha_T \Delta T$; α_T is the coefficient of thermal expansion at sea surface conditions and ΔT is chosen to be 0.5°C [*Siegel et al.*, 1995].

The 1994-1996 seawater and atmospheric pCO_2 data originate from the carbon dioxide measurements obtained from the R/V Weatherbird II in the Sargasso Sea [*Bates et al.*, 1998a; *Bates et al.*, 1998b; *Bates et al.*, 1998c]. Most of these data sets were obtained interactively via the web-based data extractor maintained by BBSR (Bermuda Biological Station for Research, Inc.; www.bbsr.edu/cintoo/bats/bats.html). The eddy-induced vertical velocity time series was obtained from the divergence of the mesoscale eddy

velocity field derived geostrophically from the merged TOPEX/Poseidon-European Remote Sensing Satellite (ERS), 0.25°, 10-day sea-surface height anomaly (SSHA) grids [AVISO, 1997]. The SSHA data were obtained via anonymous ftp from the AVISO data distribution server (ftp://ftp.cls.fr/pub/oceano/AVISO). The wind speed time series required for the gas transfer formulation was obtained from the Bermuda Airport weather station. The gridded winds to calculate the Ekman pumping vertical velocity, and cloud cover data to calculate surface PAR, were obtained from the NCEP/NCAR Reanalysis Project [*Kalnay et al.*, 1996] daily products, extracted from the Lamont-Doherty Earth Observatory (LDEO) web-based data library (ingrid.ldeo.columbia.edu/SOURCES/).

3. Model Description

The model evolved from a four-component ecosystem model [*McClain et al.*, 1996] applied to the study of physical and biological processes at Ocean Weather Station P (OWS P). There have been three upgrading stages of development for the model since the *McClain et al.* [1996] version. The first enhancement was conducted for the equatorial Pacific Warm Pool, which included a spectral formulation for the downwelling irradiance, nitrification of NH_4^+ to NO_3^-, and allowed physical forcing from offline coupling to a three-dimensional ocean circulation model simulation [*McClain et al.*, 1999]. The second improvement expanded the original Ocean Weather Station (OWS) P study [*Signorini et al.*, 2001] to include additional state variables (TCO_2, O_2, DOC, and Fe) and added a carbonate chemistry sub-model to calculate mixed-layer pCO_2 concentrations. The model was also upgraded to include air-sea gas exchange algorithms featuring five different user-selected formulations: *Monahan and Spillane* [1984], *Liss and Merlivat* [1986], *Tans et al.* [1990], *Wanninkhof* [1992], and *Wanninkhof and McGillis* [1999]. We will discuss the influence of gas exchange formulations on the model performance in the forthcoming validation section. The fourth, and most recent, version was implemented for this study and consists of additional state variables (phosphate, dissolved organic carbon, dissolved organic nitrogen, and dissolved organic phosphorus) specifically implemented in the model for the Sargasso Sea application. In addition, we implemented a light-dependent Chl:N diagnostic ratio (in mg of Chl/mmol N) to account for photoadaptation following the parameterization of *Doney et al.* [1996]:

$$\begin{aligned} &\text{Chl:N}=\text{Chl:N}_*^{max}-(\text{Chl:N}_*^{max}-\text{Chl:N}_0)\frac{I_{par}}{I_*}, I_{par}\le I_* \\ &\text{Chl:N}=\text{Ch:N}_0, \quad I_{par}>I_* \end{aligned} \qquad (1)$$

where Chl:N_*^{max} =2.0, Chl:N_0 = 1.0, and I_*=15 W m^{-2}. These selected values provide the best agreement between the BATS chlorophyll record and the model prediction. The diagnostic chlorophyll values (Chl = P Chl:N) are used to determine the depth attenuation of I_{par}.

The model of *Gregg and Carder* [1990] is used to compute the clear sky irradiance in the PAR spectrum (350-700 nm). The model is extended to include shorter wave lengths (280-700 nm) given the solar constants and ozone absorption coefficients for those wavelenghts. Cloud cover and meteorological parameters required by the spectral surface irradiance model were obtained from the NCEP/NCAR reanalysis products. The clear sky irradiance is modified to account for the observed cloud cover by applying a power law correction (*McClain et al.*, 1996) tuned to yield the observed climatological monthly mean surface irradiances (*Dobson and Smith*, 1988). Figure 1 shows a comparison between model and observed surface PAR. The observed values are from 82 cruises taken near Bermuda from 1992 to 1997 (D. Siegel personal communication). The differences between model and observed surface PAR are attributed to small-scale cloudiness variability not captured by the coarse resolution of the NCEP/NCAR reanalysis products (~2° resolution). The water column downwelling irradiance is exponentially attenuated by absorption spectra for water [*Baker and Smith*, 1982] and chlorophyll [*Dupouy et al.*, 1997].

We also introduced a quadratic formulation [*Steele and Henderson*, 1992; *Steele and Henderson*, 1995] for zooplankton mortality in the model, $(g + hZ)Z$, which provides a more realistic control of the predator abundance and phytoplankton concentration at BATS.

3.1 Governing Equations and Parameterization

The current model features the following system of coupled differential equations to simulate the dynamics of phytoplankton nitrogen (P), microzooplankton nitrogen (Z), ammonium (NH_4), nitrate (NO_3), phosphate (PO_4), dissolved organic matter (labile DOC, DON, and DOP), total carbon dioxide (TCO_2), and oxygen (O_2) stocks within the upper ocean (surface to 350 meters):

$$\frac{\partial P}{\partial t} + w_e \frac{\partial P}{\partial z} + \frac{\partial S_P P}{\partial z} - \frac{\partial}{\partial z}\left[K_v \frac{\partial P}{\partial z} \right] = (G - m - r_P)\, P - I\, Z \quad (2)$$

$$\frac{\partial Z}{\partial t} + w_e \frac{\partial Z}{\partial z} - \frac{\partial}{\partial z}\left[K_v \frac{\partial Z}{\partial z} \right] = (1-\gamma) I\, Z - (g + h\, Z) Z - r_Z\, Z \quad (3)$$

$$\frac{\partial \mathrm{NH_4}}{\partial t} + w_e \frac{\partial \mathrm{NH_4}}{\partial t} - \frac{\partial}{\partial z}\left[K_v \frac{\partial \mathrm{NH_4}}{\partial z} \right] = (a_P\, m + r_P - \pi_1\, G)\, P + \left[a_Z (g + h\, Z) + r_Z + c_{pel}\, \gamma\, I \right] Z - A_n + k_{rc}\, \mathrm{DON} \quad (4)$$

$$\frac{\partial \mathrm{PO_4}}{\partial t} + w_e \frac{\partial \mathrm{PO_4}}{\partial t} - \frac{\partial}{\partial z}\left[K_v \frac{\partial \mathrm{PO_4}}{\partial z} \right] = \left[(a_p m + r_p - G)P + (a_z (g + hZ) + r_z + c_{pel} \gamma I) Z \right] \left(\frac{\mathrm{P}}{\mathrm{N}} \right)_{\mathrm{Red}} + k_{rp}\, \mathrm{DOP} \quad (5)$$

$$\frac{\partial \mathrm{NO_3}}{\partial t} + w_e \frac{\partial \mathrm{NO_3}}{\partial z} - \frac{\partial}{\partial z}\left[K_v \frac{\partial \mathrm{NO_3}}{\partial z} \right] = -\pi_2\, G\, P + A_n \quad (6)$$

$$\frac{\partial \mathrm{TCO_2}}{\partial t} + w_e \frac{\partial \mathrm{TCO_2}}{\partial z} - \frac{\partial}{\partial z}\left[K_v \frac{\partial \mathrm{TCO_2}}{\partial z} \right] = \delta(z) \frac{\mathrm{FCO_2}}{\rho} - \frac{N_P}{\rho} \left(\frac{\mathrm{C}}{\mathrm{N}} \right)_{\mathrm{Red}} \quad (7)$$

$$\frac{\partial \mathrm{O_2}}{\partial t} + w_e \frac{\partial \mathrm{O_2}}{\partial z} - \frac{\partial}{\partial z}\left[K_v \frac{\partial \mathrm{O_2}}{\partial z} \right] = \delta(z) \frac{\mathrm{FO_2}}{\rho} + \frac{N_P}{\rho} \left(\frac{\mathrm{O_2}}{\mathrm{N}} \right)_{\mathrm{Red}} \quad (8)$$

$$\frac{\partial \mathrm{DOC}}{\partial t} + w_e \frac{\partial \mathrm{DOC}}{\partial z} - \frac{\partial}{\partial z}\left[K_v \frac{\partial \mathrm{DOC}}{\partial z} \right] = (0.05GP + a_P'\, m\, P + a_Z'\, (g + h\, Z)\, Z) \left(\frac{\mathrm{C}}{\mathrm{N}} \right)_{\mathrm{Red}} - k_{rc}\, \mathrm{DOC} \quad (9)$$

$$\frac{\partial \mathrm{DON}}{\partial t} + w_e \frac{\partial \mathrm{DON}}{\partial z} - \frac{\partial}{\partial z}\left[K_v \frac{\partial \mathrm{DON}}{\partial z} \right] = (a_P' m\, P + a_Z'\, (g + h\, Z)\, Z) - k_{rn} \mathrm{DON} \quad (10)$$

$$\frac{\partial \mathrm{DOP}}{\partial t} + w_e \frac{\partial \mathrm{DOP}}{\partial z} - \frac{\partial}{\partial z}\left[K_v \frac{\partial \mathrm{DOP}}{\partial z} \right] = (a_P'\, m\, P + a_Z'\, (g + h\, Z)\, Z) \left(\frac{\mathrm{P}}{\mathrm{N}} \right)_{\mathrm{Red}} - k_{rp}\, \mathrm{DOP} \quad (11)$$

Table 1 provides a summary of the model variables and input parameter definitions and values used for the BATS site.

The fractions $(\mathrm{C/N})_{\mathrm{Red}}$, $(\mathrm{P/N})_{\mathrm{Red}}$, and $(\mathrm{O_2/N})_{\mathrm{Red}}$ follow the Redfield ratios for carbon, nitrogen, phosphorus, and oxygen ($106\mathrm{C}:16\mathrm{N}:1\mathrm{P}:138\mathrm{O_2}$). The symbol N_p denotes the net community production. The $\mathrm{TCO_2}$, labile DOC, and oxygen concentration are in gravimetric units (μmol kg^{-1}), while all the other variables are in volumetric units (mmol m^{-3}). The water density (ρ in kg l^{-1}) is calculated using the UNESCO International Equation of State (IES 80), as described in *Fofonoff* [1985], which is a function of temperature, salinity, and pressure. The Kroenecker delta ($\delta[z = 0] = 1$; $\delta[z > 0] = 0$) is used to denote that the carbon dioxide and oxygen fluxes ($\mathrm{FCO_2}$ and $\mathrm{FO_2}$, respectively) are applied at the sea-air interface only. Details of the numerical method to solve the coupled differential equations are given in *McClain et al.* [1996].

3.2. Vertical Velocity and Vertical Diffusion Formulations

The vertical velocity variability in the BATS study area is affected primarily by vertical displacements of the thermocline imparted by the migration of mesoscale eddies through the area [*McGillicuddy et al.*, 1998; *Siegel et al.*, 1999]. This eddy pumping mechanism has been demonstrated to have a significant impact on the nutrient budget at BATS [*Siegel et al.*, 1999]. We

obtained the eddy pumping vertical velocity time series for the BATS location from the divergence of the geostrophic velocity field derived from altimeter data. Using the thermal wind equations for the geostrophic velocity components, combined with the continuity equation, we get,

$$w_{eddy} = \frac{g}{f}\left[\frac{\partial}{\partial x}\left(\frac{\partial H\eta}{\partial y}\right) - \frac{\partial}{\partial y}\left(\frac{\partial H\eta}{\partial x}\right)\right] \qquad (12)$$

where g is the acceleration due to gravity, f is the Coriolis parameter, η is the SSHA, and H is the thermocline depth (~850 m).

The 10-day high resolution (0.25°) SSHA global fields were used to derive the geostrophic currents. The SSHA and currents for the mesoscale eddy field around Bermuda are shown in Figure 2 for the 10-day average periods centered on November 6, 16, 26, and December 6, 1995. Note that the region near to and north of the BATS area is populated by very energetic mesoscale eddies. In particular, the BATS site is experiencing the effects of a slow moving, anticyclonic/cyclonic eddy pair during this time period. This mesoscale eddy signature is typical of the region, which is dominated by the occurrence of westward propagating features with SSHA as large as 25 cm, Eulerian temporal scales of roughly a month, lifetimes of several months, spatial scales of ~200 km, and a propagation of ~5 cm s^{-1} [*Siegel et al.*, 1999].

Figure 3 shows time series of SSHA and vertical velocity (w_{eddy}) for the time period of April 1995 through January 2000, the longest continuous data period. The entire data set available at the time covers the period of October 22, 1992 - January 14, 2000, but with a large gap in the 10-day AVISO composites for the period of December 16, 1993 -March 31, 1995, during which the SSHA analysis was interrupted in favor of the ice and geodesy mission objectives. An uninterrupted time series of w_{eddy}, covering the period of 1990-1998, was constructed by filling the missing points with data from adjacent years. The vertical velocity profile, w(z), is parameterized bilinearly as,

$$w(z) = 0.25 w_{eddy}\frac{z}{200}, \quad \text{for } z \le 200m$$

$$w(z) = w(200) + w_{eddy}\frac{z-201}{150}, \qquad (13)$$

$$\text{for } 200m < z \le 350m$$

This bilinear profile has a break point at 200 m where $w(z) = 0.25 w_{eddy}$. At 350 $w(z)=w_{eddy}$. The 200 m transition depth follows the *Siegel et al.* [1999] empirical parameterization, i.e., below 200 meters, isopycnal displacements are related to SLA and above 200 meters the displacement is modeled as a decreasing linear profile that extrapolates to zero at the sea surface. The eddy-induced vertical velocity ranges from -3.5 to +2.5 m d^{-1} (solid line), while the Ekman-induced downwelling peaks at -0.1 m d^{-1} (dotted line). The two components of the vertical velocity were added to force the model.

The formulation for the mixed layer eddy diffusivity (K_{v*} in m^2 s^{-1}) follows *Csanady* [1982] with an adjusted transitional Reynolds number (25 instead of 16) for the BATS region. More specifically,

$$K_{v*} = \frac{u^* H_{mld}}{25}, \quad \text{for } u^* \le 0.125$$

$$K_{v*} = \frac{1}{200}\frac{u^*}{fH_{mld}}, \quad \text{for } u^* > 0.125 \qquad (14)$$

$$u^* = \sqrt{\frac{\tau}{\rho_w}}$$

where u* is the friction velocity in m s^{-1}, τ is the wind stress in N m^{-2}, ρ_w is the water density in kg m^{-3}, H_{mld} is the mixed layer depth in meters, and f is the Coriolis parameter in s^{-1}. For numerical stability purposes, the value of K_{v*} is bound within the range of 0.0001 and 0.0116 in m^2 s^{-1}.

The K_v profile is defined as

$$K_v(z) = K_{v*}, \quad \text{for } z \le H_{mld}$$

$$K_v(z) = K_{v*}\exp\left(\ln\left[\frac{K_{vb}}{K_{v*}}\right]\frac{z}{H_{mld}}\right), \qquad (15)$$

$$\text{for } z > H_{mld}$$

where K_{vb} is the maximum of 10% of K_{v*} and 0.0001 m^2 s^{-1}. The parameterizations of w(z) and $K_v(z)$ were tuned to achieve good agreement between model and observed phosphate and nitrate concentrations (below detection level near the surface during summer).

4. Model Forcing and Boundary Conditions

4.1 Physical Forcing

A continuous time series of physical forcing, consisting of daily profiles of ocean variables, daily atmospheric variables, and hourly insolation were pre-processed and assembled offline to force the ecosystem model. Some data sets have time resolutions coarser than the time resolution required by the model, such that a linear interpolation in time was required to fill the gaps. This is the case of the CTD data, which are continually obtained at the BATS site on approximately monthly intervals. Time series profiles of temperature and salinity were interpolated at 1-meter depth intervals and daily time intervals from the monthly, 2-meter resolution CTD data sets. Figure 4 shows the time series of temperature, mixed layer depth, eddy diffusivity, vertical velocity, and PAR that were used to force the model. The forcing fields were produced for the period of 1990-1998 but only 1992-1998 are shown hereafter because the first two years are considered spin-up years and therefore will not be analyzed. There are clear interannual changes in the forcing fields, most notably in the winter-spring mixed layer depths, and accordingly the penetration depth of vigorous mixing (K_v), and in the eddy-induced upwelling-downwelling events (w_e).

4.2. Biogeochemical Forcing

The Neumann boundary condition, $\partial X/\partial z=0$, is applied at both the surface and lower (350 m) model domain boundaries for P and Z. Depth-independent initial concentrations of P, Z, and NH_4 are 0.1, 0.1, and 0.0 mmol N m^{-3}, respectively. Initial profiles of NO_3, PO_4, DOC, and DON were obtained from the BATS data. The Neumann condition was applied at the surface. Since the bottom NO_3 and PO_4 concentrations are strongly correlated with temperature ($r > 0.8$), the following equations were used to prescribe daily nitrate and phosphate concentrations at the bottom boundary (350 m):

$$NO_3(350) = 52.315 - 2.676\ T(350) \quad (16)$$

$$PO_4(350) = 3.2084 - 0.168125\ T(350) \quad (17)$$

For TCO_2 and O_2, the observed winter values at the surface and at the bottom were used to construct initial linear profiles (surface TCO_2=2050 μmol kg^{-1} and bottom TCO_2=2090 μmol kg^{-1}; surface O_2=320 μmol kg^{-1} and bottom O_2=200 μmol kg^{-1}). A fixed value equal to the initial condition was applied at the lower boundary. The total alkalinity (TA) was calculated at each time step as a function of salinity following the linear relationship given by *Bates et al.* [1996]:

$$TA = -47.155 + 66.576\ S,\ r^2 = 0.91 \quad (18)$$

The following formulations for the CO_2 and O_2 gas exchanges were applied in the form of flux boundary conditions (FCO_2 and FO_2 in mmol m^{-2} d^{-1}) at the sea-air interface:

$$FCO_2 = \rho\ K_o\ \alpha\ \Delta pCO_2 \quad (19)$$

$$FO_2 = \rho\ K_o (O_2^{sat} - O_2) \quad (20)$$

where K_o is the piston velocity, in m d^{-1}, which is a function of water temperature and wind speed (*Wanninkhof*, 1992; *Liss and Merlivat*, 1986), α is the CO_2 solubility in seawater (in mol kg^{-1} atm^{-1}, or μmol kg^{-1} μatm^{-1}) which is a function of temperature and salinity (*Weiss and Price*, 1980, Table VI), ΔpCO_2 (in μatm) is the difference between air and sea pCO_2, and O_2^{sat} is the oxygen saturation concentration (in μmol kg^{-1}) in seawater which is a function of temperature and atmospheric pressure (*Weiss*, 1970). The seawater density, ρ, is used to convert the flux into volumetric units.

The 10-year atmospheric pCO_2 time series used to force the model is based on a least-squares fit to the 2.5 years (mid 1994 to December 1997) of automated underway pCO_2 measurements in the vicinity of the BATS site (*Bates et al.*, 1998d). The slope and intercept of the long-term (secular) trend is a fit to the Mauna Loa data with slight adjustments to match the interannual pCO_2 trend of the short record at BATS. The pCO_2 time series is given by:

$$pCO_2^{air} = A_o + A_1 t + A_2 \sin\left(\frac{2\pi t}{12} + A_3\right) + A_4 \sin\left(\frac{2\pi t}{6} + A_5\right) + A_6 \sin\left(\frac{2\pi t}{4} + A_7\right) \quad (21)$$

where t is the time in months (from January 1, 1951), Ao = 282.6 μatm is the intercept, A_1= 0.125 μatm $month^{-1}$ is the slope, the amplitudes (A_2, A_4, A_6) are -7.18, -0.99, and -0.80 μatm, respectively. The phases (A_3, A_5, A_7) are 0.86, 0.28, and 0.06 radians,

respectively. Figure 5 shows the 1992-1998 time series of air pCO_2 used to force the model, and the 2.5 years (1994-1996) of observed daily-averaged air pCO_2 obtained from underway 30-minute measurements (*Bates et al*, 1998a; *Bates et al*, 1998b; *Bates et al*, 1998c).

The mixed layer pCO_2 is calculated as a function of temperature, salinity, dissolved inorganic carbon, and alkalinity following the carbonate chemistry approach outlined in *Signorini et al.* [2001]. The TCO_2 concentration depends on the balance between air-sea CO_2 flux, the biological uptake of carbon, and the vertical influx of TCO_2 through the bottom boundary. The biological uptake of carbon is performed via the net community production, N_p, which consists of the sum of all sources and sinks in the ammonium and nitrate pools. From (4) and (5) we can write

$$N_p = G\,P - (a_p\,m + r_p)P - \left[a_z\left(g + h\,Z\right) + r_z + c_{pel}\,\gamma\,I\right]Z - k_{rc}\,\mathrm{DOC}\left(\frac{\mathrm{N}}{\mathrm{C}}\right)_{\mathrm{Red}} \qquad (22)$$

Equation (22) is applied to the TCO_2 and O_2 equations ((7) and (8)), after multiplication by the corresponding Redfield ratios, as a biological sink and source of DIC and oxygen, respectively.

5. Model Validation

5.1 Gas Exchange Formulation

As stated in Section 3, sensitivity tests were conducted using five different gas exchange formulations. Figure 6 provides a comparison of 5 published air-sea gas transfer formulations. The piston velocity was converted to m yr^{-1} to conform with the original units (mol m^{-2} yr^{-1} μatm^{-1}) of the *Tans et al.* [1990] gas transfer coefficient, which is independent of solubility and Schmidt number. The comparison is made at constant salinity (36.0) and temperature (20°C). The behavior of the algorithms is quite different, which is exacerbated at wind speeds greater than 10 m s^{-1}. However, within the range of 4 to 11 m s^{-1}, the *Tans et al.* [1990] and *Wanninkhof* [1992] algorithms are very similar.

Table 2 summarizes the results of the five sensitivity tests using the gas exchange formulations shown in Figure 6. The table shows the mean value and range of the sea-air flux (FCO_2), a comparison between model and data ΔpCO_2 and TCO_2 ranges with error in percent, and the bias and root-mean-square (rms) error for the TCO_2 model prediction. The results of Table 2 show that the *Wanninkhof* [1992] algorithm provides the smallest errors for the prediction of ΔpCO_2 range and the least TCO_2 bias (+2.5% and -0.01 μmol kg^{-1}, respectively). The *Monahan and Spillane* [1984] algorithm does not match the observed pCO_2 and TCO2 ranges as well as the other four. In view of these results, we adopted the *Wanninkhof* [1992] algorithm for the air-sea gas transfer in the model. Figure 7 shows time series of predicted and observed TCO_2 and ocean pCO_2. There is very good agreement with the observed values. Monthly time series of ΔpCO_2 and FCO_2 for 1995-1996 are shown in Figure 8. The black dots connected with solid lines are based on observations. The ΔpCO_2 values are based on underway air and ocean pCO_2 measurements (*Bates et al.*, 1998a; *Bates et al.*, 1998b; *Bates et al.*, 1998c). The FCO_2 is calculated from the observed ΔpCO_2 and gas transfer coefficient from the model simulation. The dashed lines are the ΔpCO_2 and FCO_2 model predictions for the same time period. Phase and amplitude of model predictions agree well with the observed values. To compare model and observed mean values for 1995-1996, one must first eliminate January and December 1995, and January 1996, from the mean, as there are no observed ΔpCO_2 values for these 3 months. After doing that, the ΔpCO_2 and FCO_2 model means for 1995-1996 are -3.8 μatm and -0.20 mol C m^{-2} yr^{-1}, respectively. These values are within 16% of the observed ΔpCO_2, and within 20% of the FCO_2 derived from the observed ΔpCO_2 and the gas transfer coefficient used in the model (-4.5 μatm and -0.25 mol C m^{-2} yr^{-1}, respectively).

5.2. Validation of Biogeochemical Parameters

Seasonal climatological profiles of predicted and observed biogeochemical parameters are shown in Figures 9 through 17. The observed data points (black dots) covering the period of 1988-1998 are sorted by season and averaged into seasonal profiles (dotted lines). The predicted seasonal climatological profiles are shown as solid lines. Inspection of Figures 9 through 17, reveals that all biogeochemical variables are in very good agreement with model predictions.

Nutrients at the BATS site are below colorimetric detection limits [*Bates et al.*, 1996] most of the year (≤ 0.05 μmol kg^{-1}). This nutrient depletion is also manifested in the model predictions as shown in the seasonal profiles of nitrate and phosphate (Figures 9 and 10). The predicted chlorophyll profiles have surface concentrations and subsurface maximum values

in winter and summer that agree well with the equivalent features exhibited by the data. These features are less comparable with the data in summer and fall where the model tends to provide higher surface chlorophyll values and shallower chlorophyll maxima. The predicted seasonal profiles of primary production, TCO_2, O_2, and DON are all within the bounds of the data. Table 3 summarizes the comparison between predicted and observed climatological averages of surface PAR and biogeochemical parameters separated into seasons and yearly averages. The predicted surface PAR is within 7% of the observed value. The model overpredicts the surface chlorophyll by 30%, mostly due to the summer-fall discrepancies. The prediction accuracy of the nitrate and phosphate concentrations (0-50 m) are hard to evaluate because the observed values are biased due to inadequate sensitivity. The annual model nitrate (0-50m and 1992-1998 averages) is almost 3 times the observed value, while the phosphate is within 13% of the observed value. The predicted primary production (0-150 m), surface TCO_2, surface O_2, surface DON, and surface DOC are within 7%, 0.2%, 0.8%, 8%, and 1.4% of the observed values, respectively.

6. Discussion

6.1 Seasonal and Interannual Variability

The seasonal variability and interannual variability of the biogeochemical parameters respond to the variability of the physical forcing. Figure 18 highlights the biogeochemical-physical interactions on a seasonal and interannual basis. This figure shows a composite time series of PAR at 50 m, mixed-layer depth (MLD), SST, surface TCO_2, surface TA, ΔpCO_2, air-sea CO_2 flux (FCO_2), net community production (N_p, negative sign denotes a drawdown in CO_2), new production, primary production, and NO_3 and PO_4 concentrations (0-50 m). Except for MLD, SST, and TA, all of the above parameters were predicted by the model. As mentioned in Section 4, TA is calculated following *Bates et al.* [1996], and the MLD and SST are derived from Hydrostation S data.

The long-term patterns of MLD and mixed-layer temperature at BATS show significant interannual fluctuations and coherent variations on longer time scales. Some of the variations in MLD also seem correlated with the El Niño-Southern Oscillation [*Michaels and Knap*, 1996]. The years of deep mixed layers in the first half of the record (1955-1980) at Hydrostation S are often coincident with an El Niño event and the years of extremely shallow mixed layers coincide with the cold events (La Niña). After 1980, this pattern seems less clear but coherent with the change in patterns of El Niños [*Michaels and Knap*, 1996]. The depth and temperature of the winter MLD play a major role in determining interannual variations in total primary and new production [*Menzel and Ryther*, 1961; *Michaels et al.*, 1994a, *Michaels et al.*, 1994b]. Figure 18 shows that, in years of deep and cold mixed layers, the mixed-layer nitrate and phosphate concentrations are significantly elevated above the concentrations in years with shallow and warm mixed layers. This interannual scenario agrees well with the data [*Michaels et al.*, 1994a]. However, since all of this near-surface nitrate and phosphorus are quickly consumed by phytoplankton, their uptake represents a minimum amount of new production. The net primary production is significantly larger, indicating that most of the required nutrients are recycled by the community. Thus the model is configured to recycle 80% of the required nutrients from organic matter released via zooplankton and phytoplankton mortality and other organic waste (zooplankton fecal pellets and excretion and phytoplankton extracellular release). The other 20% of organic matter is equally divided into DOM and POM exported from the euphotic zone. These fractions seem to be adequate judging from the good agreement between model and observed nutrient concentrations and uptake rates.

A strong seasonality is evident in the in the sea-air ΔpCO_2, with negative values in winter when SST is minimum, and positive in summer when the MLD is shallow and SST is warmest. The seasonal cycle of FCO_2 has an amplitude of ~5 mmol C m^{-2} d^{-1} with peak outgassing in summer and peak ingassing in winter. The net community production has a similar seasonal amplitude but out of phase with FCO_2. Production peaks in spring and reaches a minimum in the fall.

The seasonal variability of surface layer TA is quite large. For the period of model simulation (1992-1998), the TA ranged between a low of 2364 μmol kg^{-1} and a high of 2404 μmol kg^{-1}. A significant portion of the TA variability is due to salinity changes via the effects of evaporation and precipitation [*Bates et al.*, 1996]. The minimum TA (2364 μmol kg^{-1}) occurred on August 1998, during the peak of La Niña. This minimum TA was accompanied by the warmest SST (28.4°C), lowest surface salinity (36.23), highest pCO_2 (420 μatm), and lowest TCO_2 (2018 μmol kg^{-1}) of the period. This low TCO_2 concentration resulted from the combination of warmest SST and lowest TA, producing the minimum dissolved CO_2 concentration of the period.

Time series of vertical profiles of chlorophyll concentration, primary production, phosphate, nitrate,

zooplankton, ammonium, oxygen and total carbon dioxide are shown in Figures 19 and 20. The vertical stratification of these parameters portrays a classical scenario of an oligotrophic environment. Nutrients are depleted within the euphotic zone most of the time and there is a distinct sub-surface chlorophyll maximum, which peaks in summer-fall. There is also a seasonal pattern in the ammonium vertical stratification with sub-surface (125 m) peaks during March when the mixed layer is deepest and primary production reaches its peak. The euphotic zone oxygen concentration peaks in February-March when solubility is highest (lowest temperatures) and primary production is also highest. The seasonal pattern of TCO_2 is characterized by minimum concentration within the upper 50 m during August when the mixed layer is shallowest and near-surface temperatures reach their peak. The TCO_2 concentration increases monotonically towards the bottom (350 m) where it is set, via the boundary condition, to a concentration of ~2090 μmol kg^{-1}. Below the euphotic zone, the phosphate and nitrate concentrations exhibit an interannual pattern coherent with the physical forcing (eddy upwelling and mixing). The phosphate and nitrate below ~100 meters shows interannual changes that depend upon the degree of winter mixing (e.g., mixed layer depth), nutricline vertical displacement, and the accompanying upwelling/downwelling induced by the mesoscale eddies.

6.2. Nitrogen and Phosphorus Budgets

The climatological (1992-1998) nitrogen and phosphorus fluxes predicted by the model are illustrated in the block diagrams in Figures 21 and 22. This diagram shows the pathways within the ecosystem and the exchanges through the bottom boundary (350 m). The mean values and standard deviations (in mmol m^{-2} yr^{-1}) are shown for each of the nitrogen and phosphorus pathways. The nutrient supply at the bottom boundary is divided into a diffusive/convective component and an advection component. The effects of convective and diffusive mixing are combined because the vertical eddy diffusivity in the model effectively takes into account both mixing processes. These components have the highest interannual variability since their standard deviations are close to or larger than the mean. The upward nutrient flux through the bottom boundary is balanced by sedimentation, 334±76 mmol m^{-2} yr^{-1} for nitrate and 21±8 mmol m^{-2} yr^{-1} for phosphate. Approximately 30% of the required nutrients are transported upward via advection, the other 70% are provided by convective and diffusive processes. Convection of nutrients reaches a maximum during winter-spring when the mixed layer is deepest. Separation of the eddy-upwelling component in the model is difficult because vertical excursions of the nutricline from the passage of mesoscale eddies affect both advective and diffusive components of the nutrient flux. Therefore, the effect of eddy upwelling may be larger than 30% (advective component) and approach the ~50% reported by *Siegel et al.* [1999]. The new production predicted by the model, shown in Figure 21, nitrogen uptake of 0.47±0.14 mol N m^{-2} yr^{-1}, is within 6% of the 0.50±0.15 mol N m^{-2} yr^{-1} mean estimate for the Sargasso Sea reported by *Siegel et al.* [1999]. The predicted and estimated values are statistically identical judging from the magnitude of their individual standard deviations.

6.3. Carbon Budget

Figure 23 shows the climatological carbon balance for the BATS region based on the 7-year (1992-1998) model simulation. The two boxes in Figure 23 represent the dissolved inorganic carbon (DIC) in surface water (solubility pump), and the biological pump, which takes up CO_2 from the DIC pool via photosynthesis and exports POC and labile DOC as a byproduct. The labile DOC is quickly consumed by bacteria and remineralized into DIC. The biological DIC consumption, i.e., the net community production (2.3 mol C m^{-2} yr^{-1}), is balanced by the air-sea CO_2 flux (0.3 mol C m^{-2} yr^{-1}), the remineralization of DOC (0.9 mol C m^{-2} yr^{-1}), and the DIC flux (1.1 mol C m^{-2} yr^{-1}) at the bottom boundary (350 in). In terms of overall carbon balance, the sedimentation rate (POC + fecal pellets), 1.4 mol C m^{-2} yr^{-1}, is balanced by the air-sea CO_2 flux and the DIC advection through the bottom boundary. *Michaels et al.* [1994] calculate a POC flux of 0.4 to 1.9 mol C m^{-2} for the period April-December, based on deficits of ^{234}Th. This POC flux estimate is for 150 meters and it is based on 1988-1993 BATS data. The model POC flux (1992-1998) for the same depth and time-averaging constraints (April-December) ranges from 0.6 to 0.8 mol C m^{-2}, which is within the range of the *Michaels et al.* [1994] estimate.

7. Summary and Conclusions

An analysis of biogeochemical- physical interactions and carbon cycle was conducted for the BATS region using a combination of field observations and a one-dimensional ecosystem/carbon-cycle model. The required forcing and boundary conditions were derived from the BATS comprehensive hydrographic and biogeochemical data sets. The model performance was evaluated by comparing 10 predicted parameters

(ΔpCO_2, TCO_2, O_2, PP, PAR, Chl-a, NO_3, PO_4, DON, DOC) with available time series of equivalent parameters observed at BATS. Most model results fall within 8% of the observed values.

Primary production peaks at 657 mg C m^{-2} d^{-1} in spring and is reduced to 375 mg C m^{-2} d^{-1} in the fall. The surface nitrate and phosphate concentrations are extremely low during summer-fall (0.1-0.2 and 0.002-0.003 mmol m^{-3}, respectively). Regenerated production is set to a very high level in the model (~80% of the nutrients are recycled) in order to achieve a good match with observations, an indication of the oligotrophic nature of the BATS site. The model also shows that a first-order nitrogen balance can be achieved without resorting to nitrification processes from other species, such as cyanobacteria nitrogen fixation.

The model results reveal significant interannual variability of mixed-layer TCO_2. There was an upward trend of ~1.2 μmol kg^{-1} yr^{-1} in the surface TCO_2 during 1992-1996, which is similar to the ~1.7 μmol kg^{-1} yr^{-1} observed by *Bates et al.* [1996] during 1988-1993. They attributed this trend to the uptake of atmospheric CO_2 through gas exchange, or natural variability of the subtropical gyre. However, our model results show that this trend is reversed during 1997-1998 to -2.7 μmol kg^{-1} yr^{-1}. This relatively large TCO_2 change was accompanied by a significant drop (9 μmol kg^{-1}) in TA from 2392 μmol kg^{-1} in 1997 to 2383 μmol kg^{-1} in 1998. The minimum TA (2364 μmol kg^{-1}) occurred on August 1998, during the peak of La Niña. The drop in TA was large enough to reverse the TCO_2 trend imposed by atmospheric CO_2 uptake.

The sea-air CO_2 flux was evaluated using 5 different gas transfer coefficients. The CO_2 flux obtained with these 5 methods ranges from -0.12 to -0.50 mol C m^{-2} yr^{-1}, indicating that the BATS region is a weak sink for atmospheric CO_2. The mean CO_2 flux for 1992-1998, -0.3 mol C m^{-2} yr^{-1}, was calculated using the *Wanninkhof* [1992] gas transfer coefficient because it provides the best match of ΔpCO_2 with observations and the least TCO_2 bias (model-observation annual means). The atmospheric uptake of CO_2 is balanced by an upward bottom (350 m) flux of DIC (+1.1 mol C m^{-2} yr^{-1}) and sedimentation (-1.4 mol C m^{-2} yr^{-1}). These results show that it is possible to achieve a first-order carbon cycle balance without considering the effects of horizontal advection.

References

Archiving, Validation, and Interpretation of Satellite Data in Oceanography (AVISO), AVISO handbook: Sea level anomaly files, Publ. AVI-NT-001-312-CN, 21st ed., 24 pp., Cent. Natl. d'Etudes Spatiales, Toulouse, France, 1997.

Baker, K. S., and R. C. Smith, Bio-optical classification and model of natural waters, Limnol. Oceanogr., 27, 500-509, 1982.

Bates, N. R., A. F. Michaels, and A. H. Knap, Seasonal and interannual variability of oceanic carbon dioxide species at the U.S. JGOFS Bermuda Atlantic Time-series Study (BATS) site, Deep Sea Res. II, 43, 347-383, 1996.

Bates, N.R., Knap, A.H., Bahr, F., Benson, J., Chipman, D.W., Howse, F., Johnson, R.J., and Takahashi, T., Carbon dioxide measurements obtained aboard the R/V Weatherbird II in the Sargasso Sea, June-December 1994. Bermuda Biological Station For Research Data Report, BBSR CO_2 Data Report 98-1, Ferry Reach, Bermuda, 1998a.

Bates, N.R., Knap, A.H., Bahr, F., Benson, J., Chipman, D.W., Howse, F., Johnson, R.J., and Takahashi, T., Carbon dioxide measurements obtained from the R/V Weatherbird II in the Sargasso Sea, January-December 1995. Bermuda Biological Station For Research Data Report, BBSR CO_2 Data Report 98-2, Ferry Reach, Bermuda, 1998b.

Bates, N.R., Knap, A.H., Bahr, F., Bell, S.J., Benson, J., Howse, F.A., Chipman, D.W., and Takahashi, Carbon dioxide measurements obtained aboard the R/V Weatherbird II in the Sargasso Sea, January-December 1996. Bermuda Biological Station for Research Data Report, BBSR CO_2 Data Report 98-3, Ferry Reach, Bermuda, 1998c.

Bates, N. R., T. Takahashi, D. W. Chipman, and A. H. Knap, Variability of pCO_2 on diel to seasonal timescales in the Sargasso Sea near Bermuda, J. Geophys. Res., 103,15,567-15,585, 1998d.

Bates, N. R., Interannual variability of oceanic CO2 and biogeochemical properties in the Western North Atlantic subtropical g

Carpenter, E. J., Nitrogen fixation by marine Oscillatoria (Trichodesmium) in the world's oceans, Academic Press, New York, 1983.

Dobson, F. W., and S. D. Smith, Bulk models of solar radiation at sea, Q. J. R. Meteorol. Soc., 114, 165-182, 1988.

Doney, S. C., D. M. Glover, and R. G. Najjar, A new coupled, one-dimensional biological-physical model for the upper ocean: Applications to the JGOFS Bermuda Atlantic Time-series Study (BATS) site, Deep Sea Res. Part II 43, 591-624, 1996.

Dupouy, C., J. Neveux, and J. M. André, Spectral absorption coefficient of photosynthetically active pigments in the equatorial Pacific Ocean (165°E-150°W) Deep Sea Res. Part II, 44, 1881-1906, 1997.

Fofonoff, N. P., Physical properties of seawater: A new salinity scale and equation of state for seawater, J. Geophys. Res., 90, 3332-3342, 1985.

Ivlev, V. S., Experimental Ecology of the Feeding of Fishes, 302 pp., Pischepromazat, Moscow, 1955.

Kalnay, E., et al., The NCEP/NCAR 40-year reanalysis project, Bull. Amer. Meteor. Soc.,1996.

Liss, P. S., and L. Merlivat, Air-sea gas exchange rates: Introduction and synthesis, in The Role of Air-Sea Exchange in Geochemical Cycling, edited by P. Buat-Ménard, pp. 113-129, D. Reidel, Hingham, Mass., 1986.

McClain, C. R., K. Arrigo, K.-S. Tai, and D. Turk, Observations and simulations of physical and biological processes at ocean weather station P, 1951-1980, J. Geophys. Res., 101, 3697-3713, 1996.

McClain, C. R., R. Murtugudde, and S. R. Signorini, A simulation of biological processes in the equatorial Pacific Warm Pool at 165°E, J. Geophys. Res., 104, 18,305-18,322, 1999.

McGillicuddy Jr., D. J., A. R. Robinson, D. A. Siegel, H. W. Jannasch, R. Johnson, T. D. Dickey, J. McNeil, A. F. Michaels, and A. H. Knap, Influence of mesoscale eddies on new production in the Sargasso Sea, Nature, 394, 263-265, 1998.

Menzel, D. W., and J. H. Ryther, The annual cycle of primary production in the Sargasso Sea off Bermuda, Deep Sea Res. Part 1, 6, 351-367, 1960.

Menzel, D. W., and J. H. Ryther, Annual variations in primary production of the Sargasso Sea off Bermuda, Deep Sea Res. Part 1, 7, 282-288, 1961.

Michaels, A. F., and A. H. Knap, Overview of the U.S. JGOFS Bermuda Atlantic Time-series Study and Hydrostation S program, Deep Sea Res.II 43, 157-198, 1996.

Michaels, A. F., A. H. Knap, R. L. Dow, K. Gundersen, R. J. Johnson, J. Sorensen, A. Close, G. H. Knauer, S. E. Lohrenz, V. A. Asper, M. Tuel, and R. R. Bidigare, Seasonal patterns of ocean biogeochemistry at the U.S. JGOFS Bermuda Atlantic Time-series Study site, Deep Sea Res. Part 1, 41, 1013-1038, 1994a.

Michaels, A. F., N. R. Bates, K. O. Buesseler, C. A. Carlson, and A. H. Knap, Carbon system imbalances in the Sargasso Sea, Nature, 372, 537-540, 1994b.

Olson, R.J., S. W. Chisholm, E. R. Zettler, M. A. Altabet, and J. A. Dusenberry, Spatial and temporal distributions of prochlorophyte picoplankton in the North Atlantic Ocean, Deep Sea Res. Part 1, 37, 1033-1051, 1990a.

Olson, R.J., S. W. Chisholm, E. R. Zettler, and E. V. Armbrust, Pigments, size and distribution of Synechococcus in the North Atlantic and Pacific Oceans, Limnol. Oceanogr., 35, 45-58, 1990b.

Pocklington, R., Secular changes in the ocean off Bermuda, J. Geophys. Res., 77, 6604- 6607, 1972.

Schroeder, E., H. Stommel, D. W. Menzel, and W. J. Sutcliffe, Climatic stability of eighteen degree water at Bermuda, J. Geophys. Res., 64, 363-366, 1959.

Schroeder, E., and H. Stommel, How representative is the series of Panulirus stations of monthly mean conditions off Bermuda?, Prog. Oceanogr., 5, 31-40, 1969.

Siegel, D. A., R. Itturiaga, R. R. Bidigare, R. C. Smith, H. Pak, T. D. Dickey, J. Marra, and K. S. Baker, Meridional variations of the spring-time phytoplankton community in the Sargasso Sea, J. Mar. Res., 48, 379-412, 1990.

Siegel, D. A., A. F. Michaels, J. C. Sorensen, M. C. O'Brien, and M. A. Hammer, Seasonal variability of light availability and utilization in the Sargasso Sea, J. Geophys. Res., 100, 8695-8713, 1995.

Siegel, D. A., D. J. McGillicuddy Jr., and E. A. Fields, Mesoscale eddies, satellite altimetry, and new production in the Sargasso Sea, J. Geophys. Res., 104, 13,359-13,379, 1999.

Signorini, S. R., C. R. McClain, J. R. Christian, and C. S. Wong, Seasonal and interannual variability of phytoplankton, nutrients, TCO_2, pCO_2, and O_2 in the eastern subarctic Pacific (OWS P), J. Geophys. Res., in press, 2001.

Steele, J. H., and E. W. Henderson, The role of predation in plankton models, J. Plankton Res., 14, 157-172, 1992.

Steele, J. H., and E. W. Henderson, Predation control of plankton demography, J. Plankton Res., 52, 565-573, 1995.

Tans, P. P., 1. Y. Fung, and T. Takahashi, Observational constraints on the global atmospheric CO2 budget, Science, 247, 1431-1438, 1990.

Wanninkhof, R., Relashionship between wind speed and gas exchange over the ocean, J. Geophys. Res., 97, 7373-7382, 1992.

Wanninkhof, R., and W. R. McGillis, A cubic relationship between air-sea CO2 exchange and wind speed, Geophys. Res. Lett., 26, 1889-1892, 1999.

Weiss, R. F., and B. A. Price, Nitrous oxide solubility in water and seawater, Mar. Chem., 8, 347-359, 1980.

Wunsch, C., Bermuda sea level in relation to tides, weather, and baroclinic fluctuations, Rev. Geophys. Space Phys., 10, 1-49, 1972.

Table 1. Model variables and input parameters. For variables (P, Z, NH_4, NO_3, DON, DOC, DOP, TCO_2, and O_2), the column of values contains initial mixed-layer concentrations values (for DON, DOC, DOP, TCO_2, and O_2, bottom concentration values are also provided). The remaining values are the values assigned to the various model parameters.

Symbol	Value	Definition
P	0.1/0.1	Phytoplankton concentration (mmol N m^{-3})
Z	0.1/0.1	Zooplankton concentration (mmol N m^{-3})
NH_4	0.0/0.0	Ammonium concentration (mmol m^{-3})
NO_3	0.2/4.0	Nitrate concentration (mmol m^{-3})
PO_4	0.01/0.20	Phosphate concentration (mmol m^{-3})
DON	1.0/0.0	Labile dissolved organic nitrogen (mmol m^{-3})
DOC	17.0/0.0	Labile dissolved organic carbon (μmol kg^{-1})
DOP	0.039/0.0	Labile dissolved organic phosphorous (mmol m^{-3})
TCO_2	2050/2090	Total dissolved inorganic carbon (μmol kg^{-1})
O_2	320/200	Oxygen concentration (μmol kg^{-1})
π_1	...	Regenerated production fraction, Dimensionless
π_2	...	New production production fraction, Dimensionless
K_{NO3}	0.024	Half saturation for nitrate uptake (mmol m^{-3})
K_{NH4}	0.024	Half saturation for ammonium uptake (mmol m^{-3})
m	0.05	Phytoplankton mortality rate (d^{-1})
G_o	0.5899	Phytoplankton growth rate at 0°C (d^{-1})
k_{gp}	0.0633	Temperature sensitivity of algal growth ($^oC^{-1}$)
pk	5	Ammonium inhibition of nitrate uptake, Dimensionless
S_{max}	0	Maximum phytoplankton sinking rate (m d^{-1})
g	0.12	Linear coefficient of zooplankton mortality (d^{-1})
h	0.30	Quadratic coefficient of zooplankton mortality ($mmol^{-1}$ m^3 d^{-1})
I	...	Herbivore grazing term, $I = R\Lambda P[1 - exp(-\Lambda P)]$, ($d^{-1}$)
R	7.0	Maximum grazing rate (d^{-1})
Λ	2.0	Herbivore grazing constant (m^3 mmol N^{-1})
γ	0.3	Unassimilated zooplankton ingestion ratio, Dimensionless
r_{zo}	0.019	Respiration rate for zooplankton at 0°C (d^{-1})
k_{rz}	0.08	Temperature sensitivity of zooplankton respiration ($^oC^{-1}$)
a_p	0.8	Fraction of dead phytoplankton converted to ammonium, Dimensionless
a_z	0.8	Fraction of dead zooplankton converted to ammonium, Dimensionless
a'_p	0.1	Fraction of dead phytoplankton converted to DOC, DON, and DOP, Dimensionless
a'_z	0.1	Fraction of dead zooplankton converted to DOC, DON, and DOP, Dimensionless
k_{rc}	0.00005	Remineralization rate of DOC (d^{-1})
k_{rn}	0.0001	Remineralization rate of DON (d^{-1})
k_{rp}	0.0001	Remineralization rate of DOP (d^{-1})
$A^n{}_{max}$	2.0	Maximum rate of nitrification (mmol N d^{-1})
D_{min}	0.0095	Minimum inhibition dosage for nitrification (W m^{-2})
K_D	0.036	Half saturation dosage for nitrification photoinhibition (W m^{-2})
c_{pel}	0.8	Fecal pellet remineralization fraction, Dimensionless

Table 2. Mean sea-air CO_2 flux (FCO_2), mean range of sea-air CO_2 flux, and error analysis for model-predicted ocean ΔpCO_2 and TCO_2 using five gas transfer coefficients (K) and BATS site observations as a reference. Data availability limits the ΔpCO_2 model-data comparison to 1995-1996 and the TCO_2 model-data comparison to 1992-1997. The TCO_2 bias is defined as the difference between the model and observed means for 1992-1998. The RMS error is also calculated for 1992-1998.

	FCO_2, mol m^{-2} yr^{-1}		ΔpCO_2 Range, μatm			TCO_2 Range, μmol kg^{-1}			TCO_2, μmol kg^{-1}	
	Mean	Range	Model	Data	Error	Model	Data	Error	Bias	RMS
K_1	-0.50	3.93	91.7	94.2	-2.7%	37.8	46.2	-18%	+0.62	±8.0
K_2	-0.44	3.40	96.6	94.2	+2.5%	33.5	46.2	-28%	-0.01	±8.0
K_3	-0.32	2.12	104.8	94.2	+11.2%	26.4	46.2	-43%	-1.02	±8.9
K_4	-0.40	3.17	103.8	94.2	+10.1%	28.0	46.2	-39%	+0.85	±8.8
K_5	-0.12	0.79	107.7	94.2	+14.3%	21.2	46.2	-54%	-5.48	±11.6

The gas exchange formulations used in the analysis are: K_1=*Tans et al.* [1990]; K_2=*Wanninkhof* [1992]; K_3=*Liss and Merlivat* [1986]; K_4=*Wanninkhof and McGillis* [1999]; and K_5=*Monahan and Spillane* [1984].

Table 3. Summary of seasonal and climatological comparisons between predicted and observed biogeochemical parameters. The climatological values from the data are based on 1988-1998 averages, while those obtained from the model are based on 1992-1998 averages.

	Winter		Spring		Summer		Fall		Year	
	Model	Data	Model	Data	Model	Data	Model	Data	Model	Data
PAR	46.0	49.3	83.5	89.8	96.3	99.2	61.5	68.9	71.8	76.8
Chl-*a*	0.14	0.16	0.14	0.11	0.11	0.04	0.12	0.07	0.13	0.10
NO_3	0.43	0.16	0.64	0.11	0.16	0.06	0.09	0.16	0.33	0.12
PO_4	0.012	0.009	0.017	0.003	0.002	0.010	0.003	0.008	0.009	0.008
PP	456.3	432.4	656.5	593.5	440.4	381.8	375.0	387.3	482.1	448.8
DON	0.94	0.94	0.88	1.05	0.97	1.10	1.00	1.03	0.95	1.03
DOP	0.06	...	0.05	...	0.06	...	0.06	...	0.06	...
DOC	14.0	12.9	13.1	13.1	14.4	15.3	14.4	15.5	14.0	14.2
TCO_2	2049.4	2046.2	2058.1	2055.3	2036.9	2035.5	2030.4	2024.1	2043.7	2040.3
O_2	223.2	218.0	223.7	223.8	207.2	206.0	208.3	206.9	215.6	213.7

Nitrate, phosphate, labile DON, DOP (mmol/m^3), and DOC (μmol kg^{-1}) were averaged from surface to 50 m. The Chl-*a* (mg/m^3), TCO_2, O_2 (μmol kg^{-1}) concentrations are surface values. The observed surface irradiance (PAR[O^-]), in W m^{-2}, is obtained from 1992-1997 averages. The primary production (PP in mg C m^{-2} d^{-1}) is integrated from surface to 150 m for the period of 1992-1997.

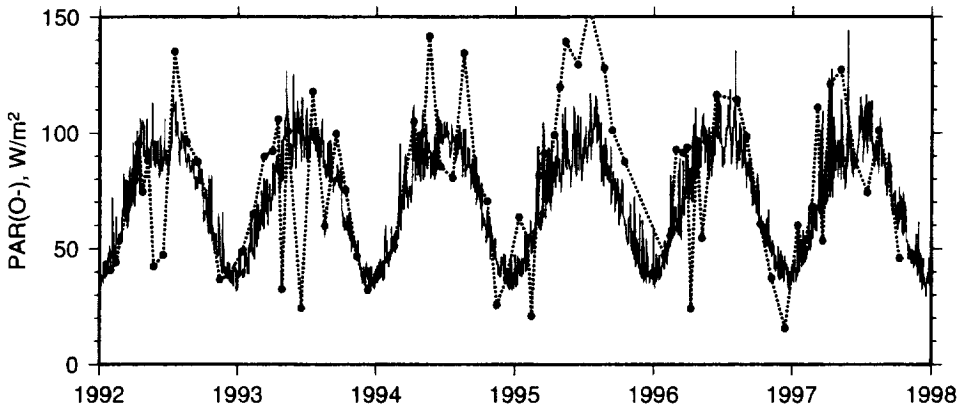

Figure 1: Comparison between model and observed daily averaged surface PAR (just below the surface at ~1 m) for 1992-1997. The solid line is the model time series while the black circles connected by the dotted line are the observed values.

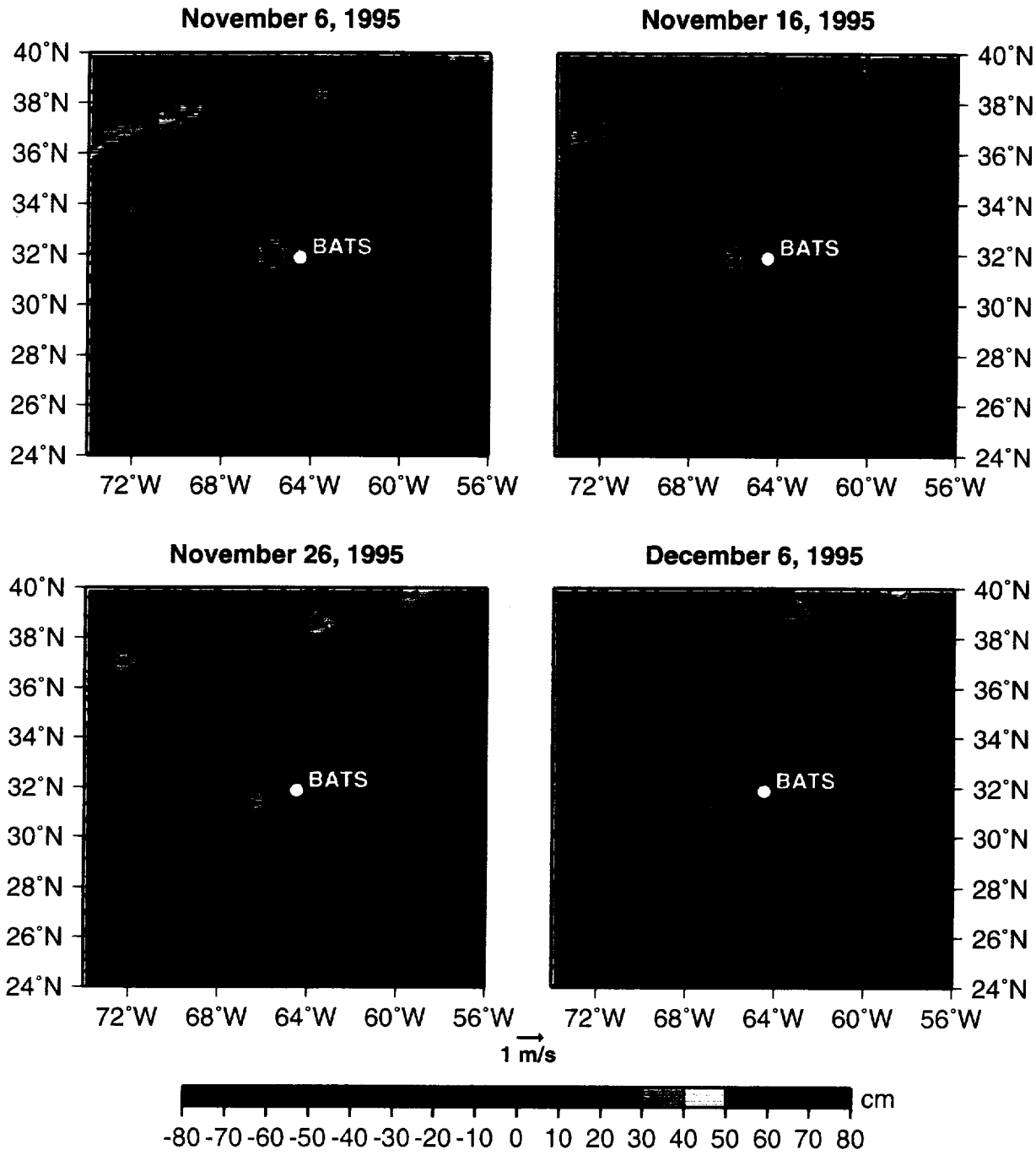

Figure 2: Sea surface height anomaly (cm) and geostrophically derived currents near the BATS site for four 10-day composites in November-December 1995. Note the two mesoscale eddies, one cyclonic and one anticyclonic, fringing the BATS site (white circle).

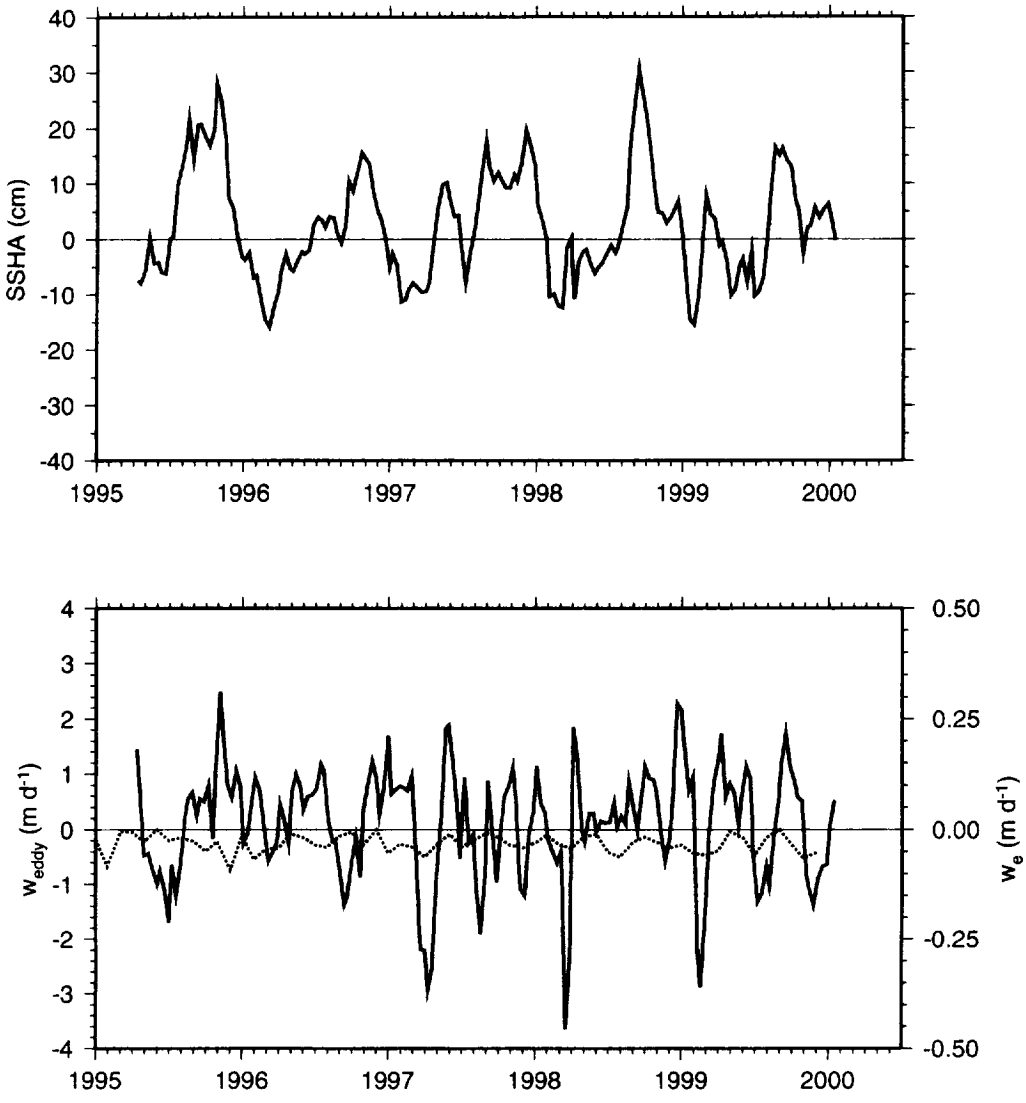

Figure 3: Time series of SSHA (top) and Ekman (w_e, dotted line) and eddy-induced (w_{eddy}, solid line) vertical velocities (bottom).

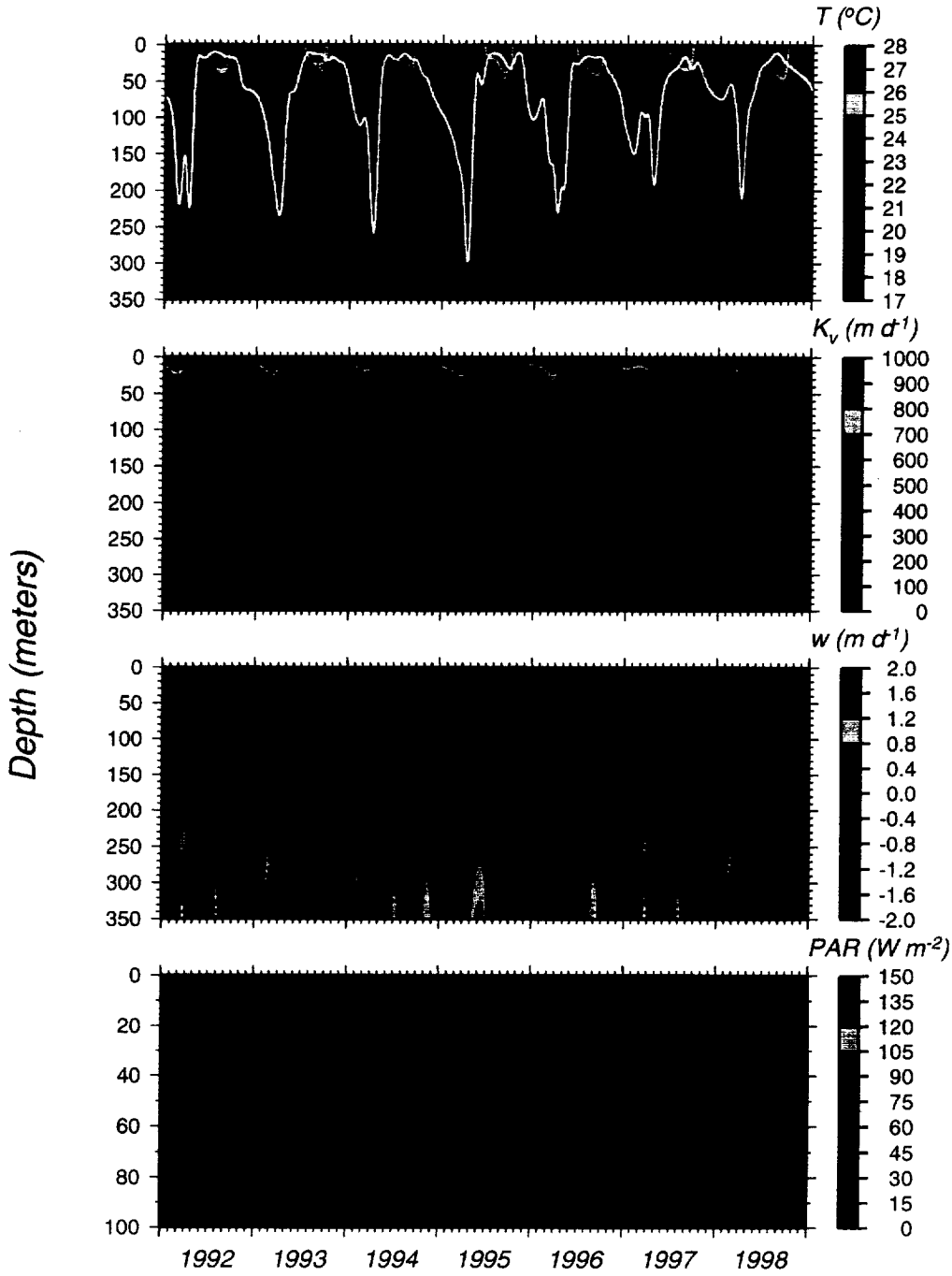

Figure 4: Time series of temperature (T), mixed layer depth (white line), vertical eddy diffusivity (K_v), vertical velocity (w), and PAR for the period of 1992-1998.

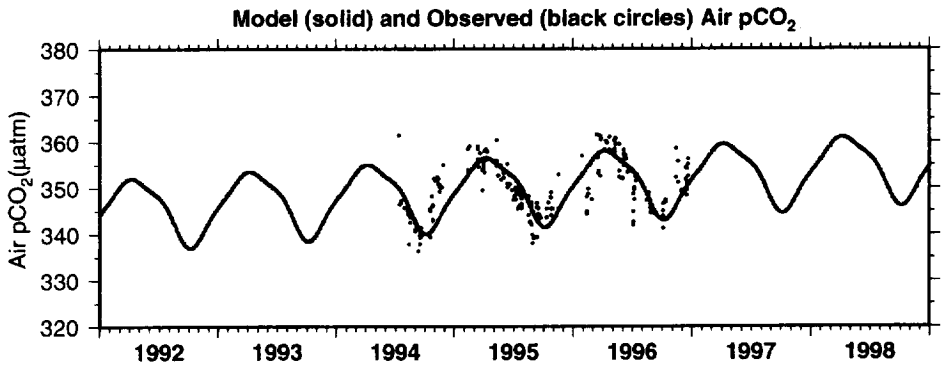

Figure 5: Time series of air pCO_2 for 1992-1998. The thick line denotes the time series used to force the model. The black circles are daily-averaged air pCO_2 values obtained from underway 30-min measurements (*Bates et al.*, 1998a, 1998b, 1998c).

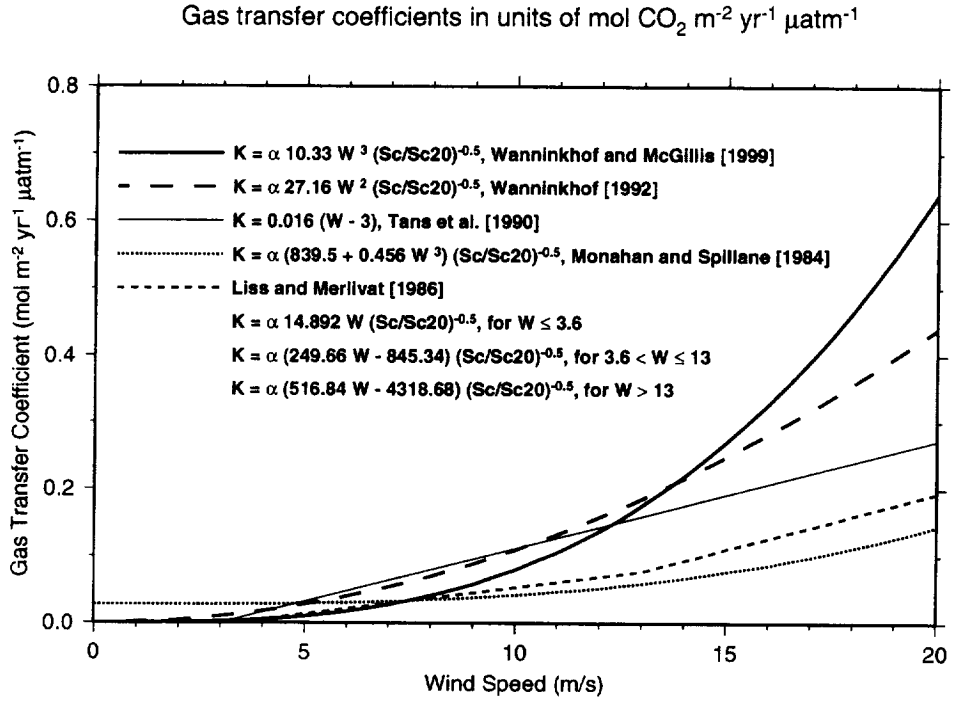

Figure 6: Gas transfer coefficient as a function of wind speed. Curves are shown for five different formulations. All constants have been converted to reflect units of mol CO_2 m^{-2} yr^{-1} μatm^{-1}, which are the units of the *Tans et al.* [1990] formulation. The assumptions are: SST=20°C and SSS=36, so that the CO_2 solubility $\alpha=3.223\times10^{-5}$ mol m^{-3} μatm^{-1} and the Schmidt number ratio $(S/Sc20)^{-0.5}=1.0$.

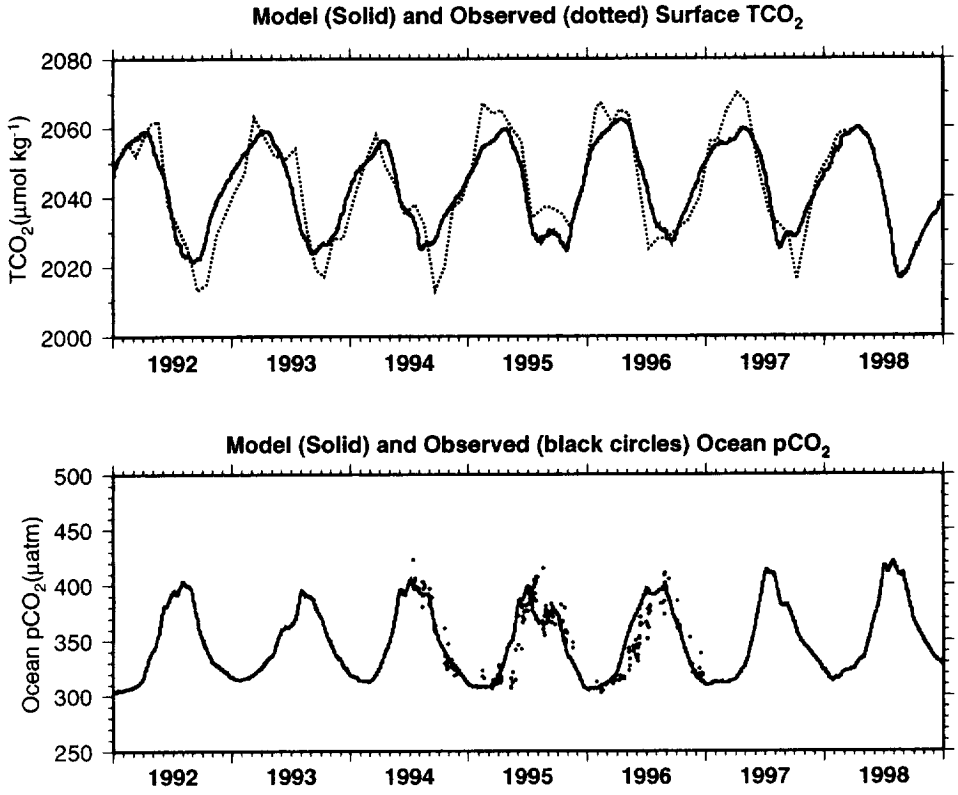

Figure 7: Time series of TCO_2 and ocean pCO_2 for 1992-1998. The thick lines denote model predictions. The observed TCO_2 (1992-1997) is shown by the dotted line. The black circles are daily-averaged ocean pCO_2 values obtained from underway 30-min measurements (*Bates et al.*, 1998a, 1998b, 1998c).

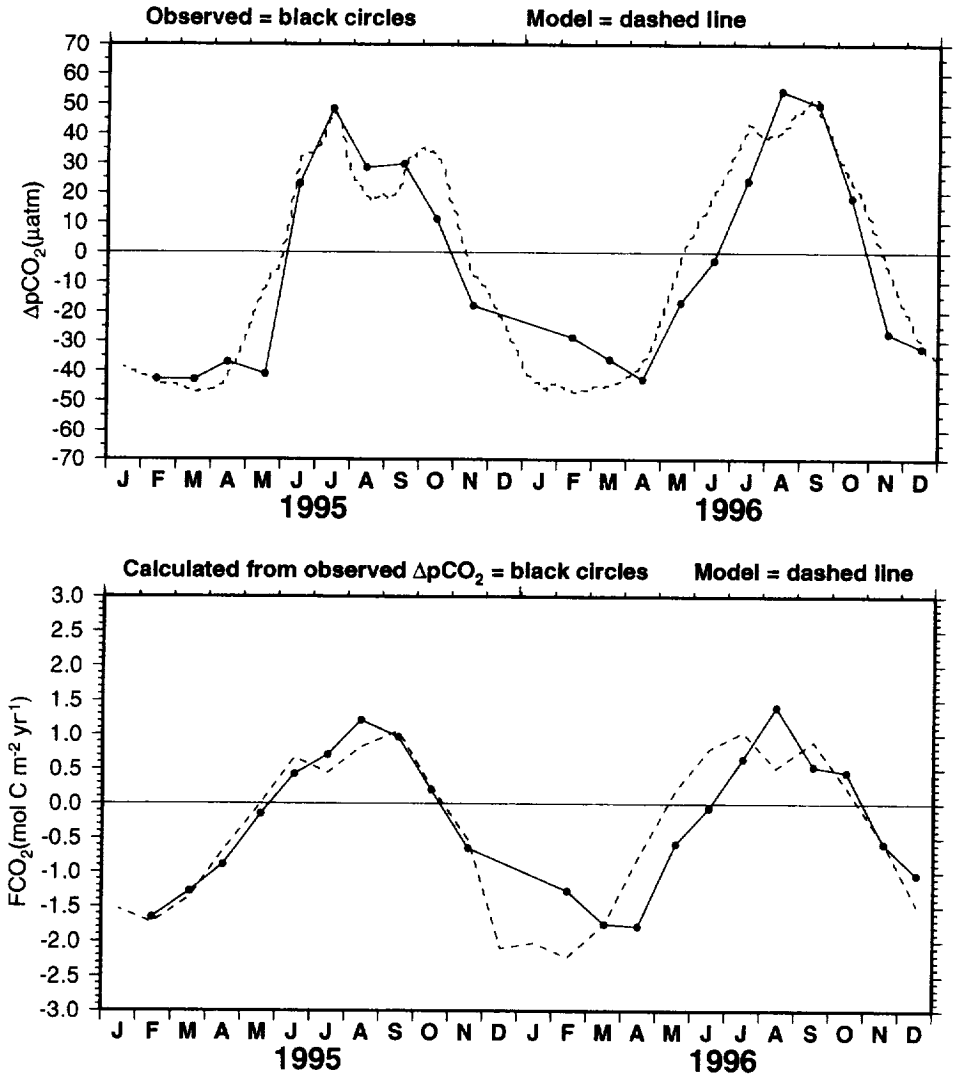

Figure 8: Monthly time series of ΔpCO_2 (top panel) and sea-air CO_2 flux (FCO_2, bottom panel) for 1995-1996. The black dots connected with solid lines are based on observations. The ΔpCO_2 values are based on underway air and ocean pCO_2 measurements (*Bates et al.*, 1998). The FCO_2 is calculated from the observed ΔpCO_2 and gas transfer coefficient from the model simulation. The dashed lines are the model predictions for the same time period.

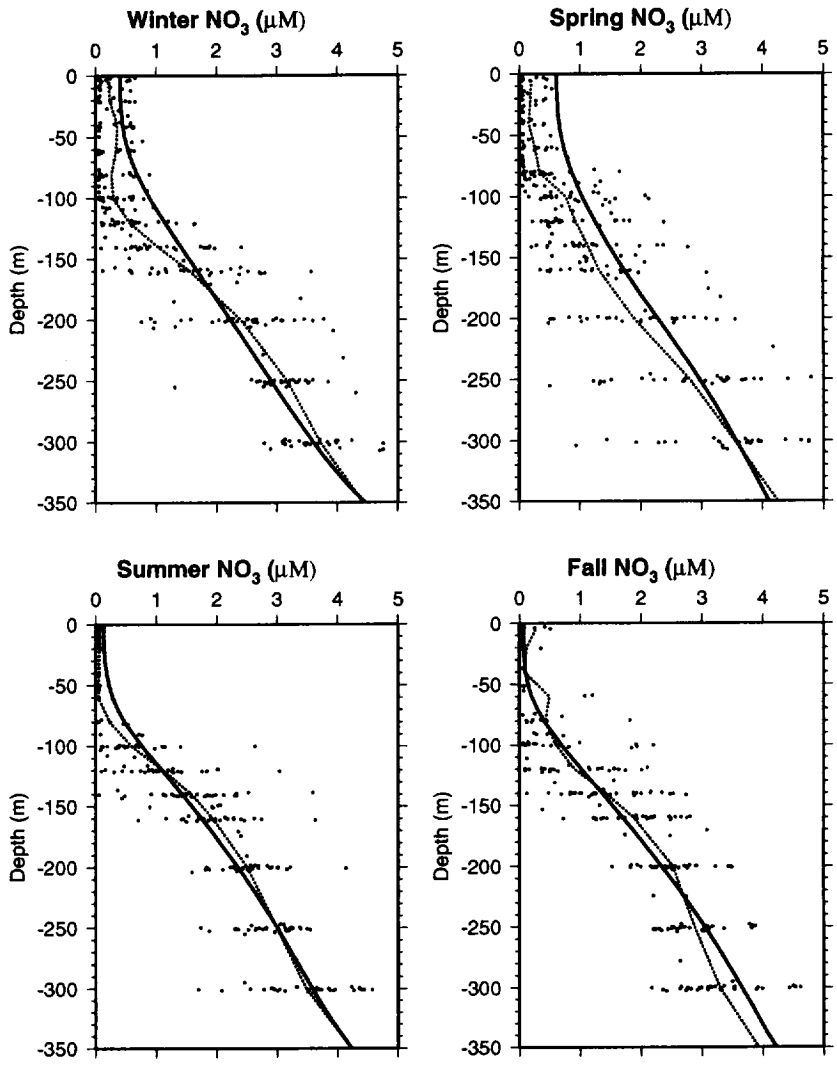

Figure 9: Climatological profiles of nitrate for winter, spring, summer, and fall. The solid lines represent model profiles (1992-1998). The dots show all data points available within the 1988-1998 time period and the dotted lines are the climatological data averages.

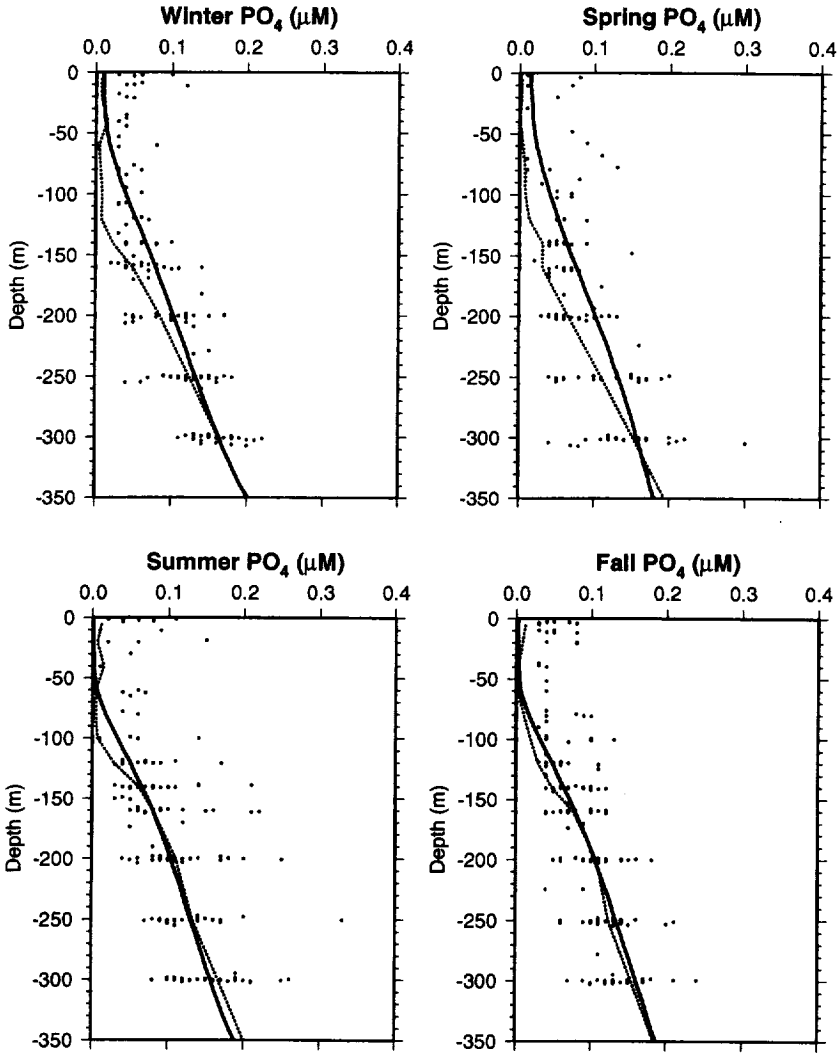

Figure 10: Same as in Figure 9, except for winter, spring, summer, and fall phosphate.

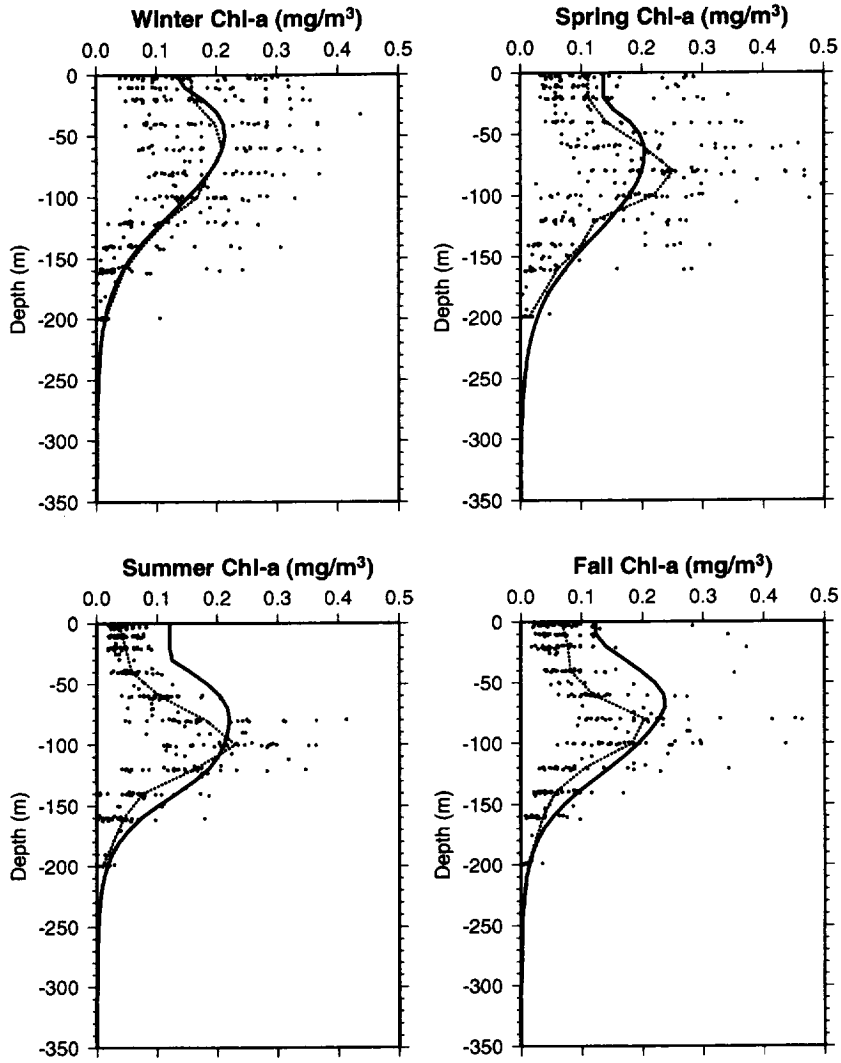

Figure 11: Same as in Figure 9, except for winter, spring, summer, and fall chlorophyll-*a*.

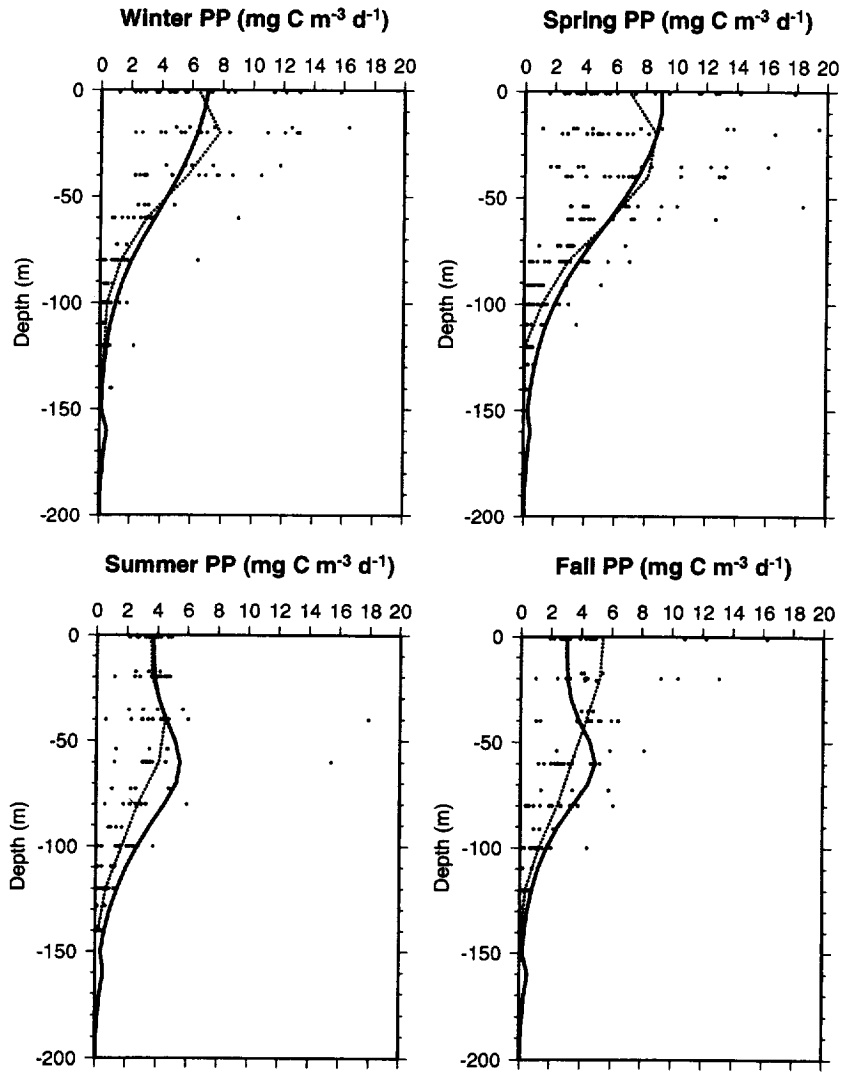

Figure 12: Same as in Figure 9, except for winter, spring, summer, and fall primary production.

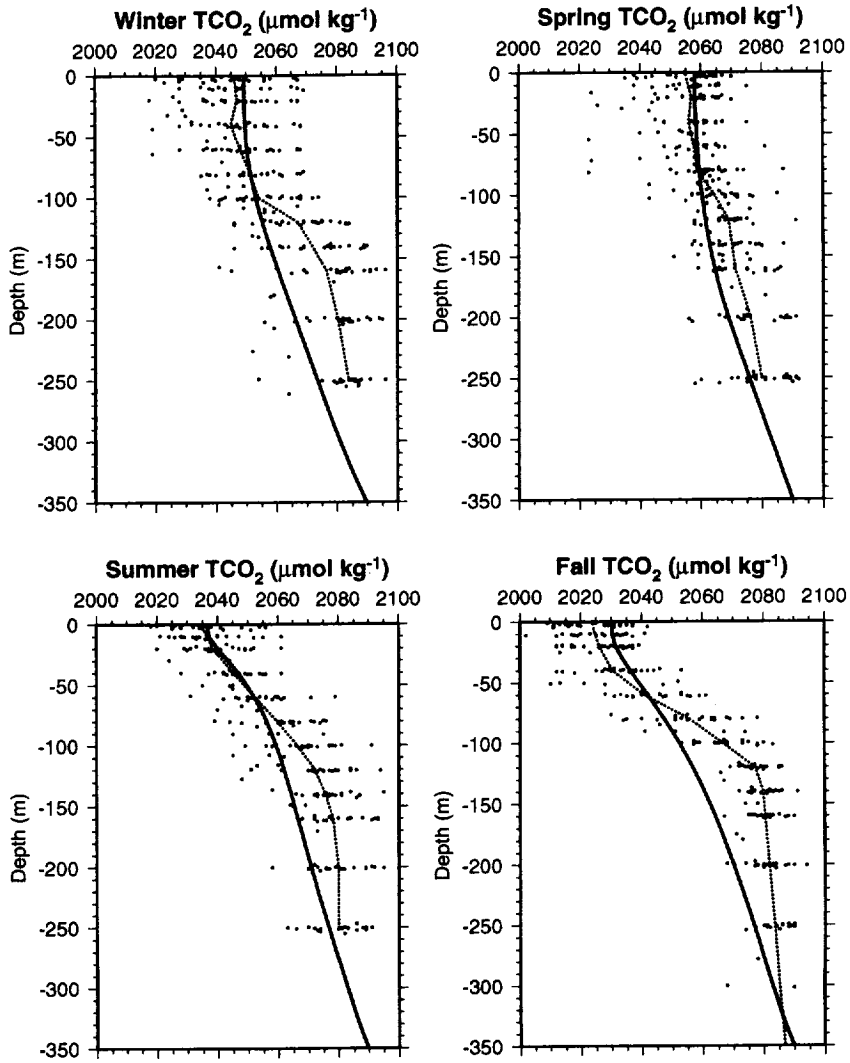

Figure 13: Same as in Figure 9, except for winter, spring, summer, and fall total carbon dioxide.

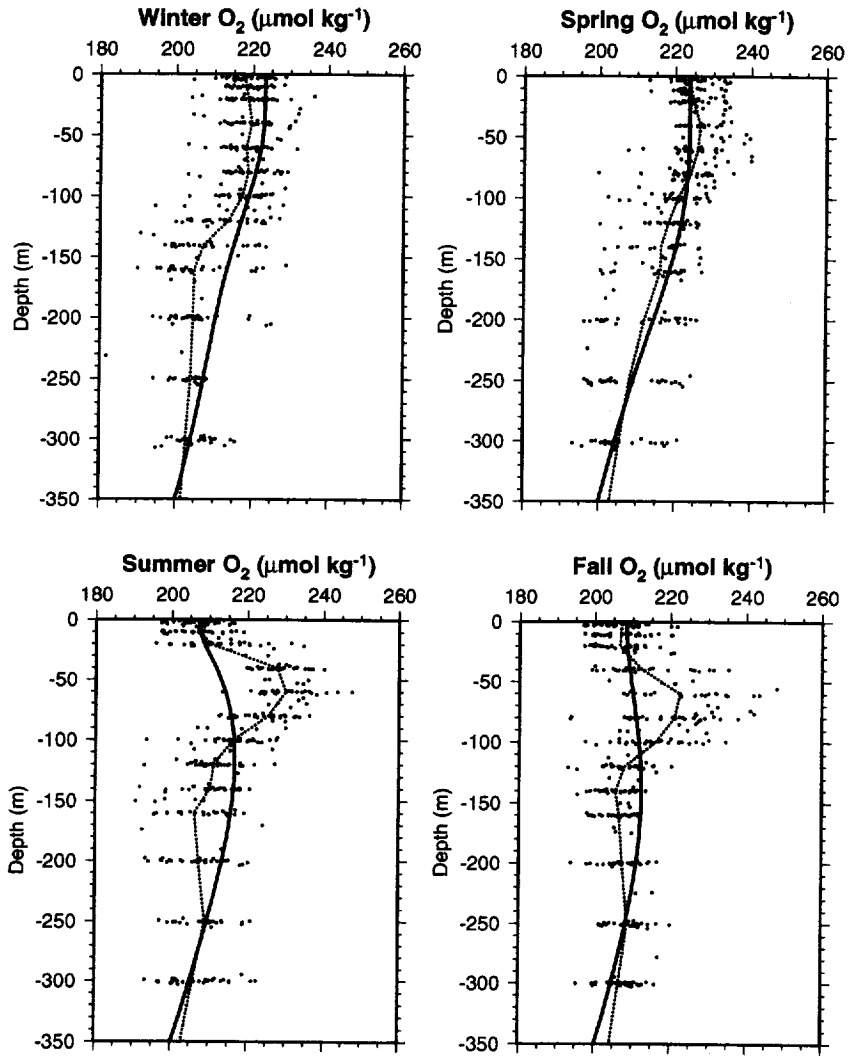

Figure 14: Same as in Figure 9, except for winter, spring, summer, and fall oxygen.

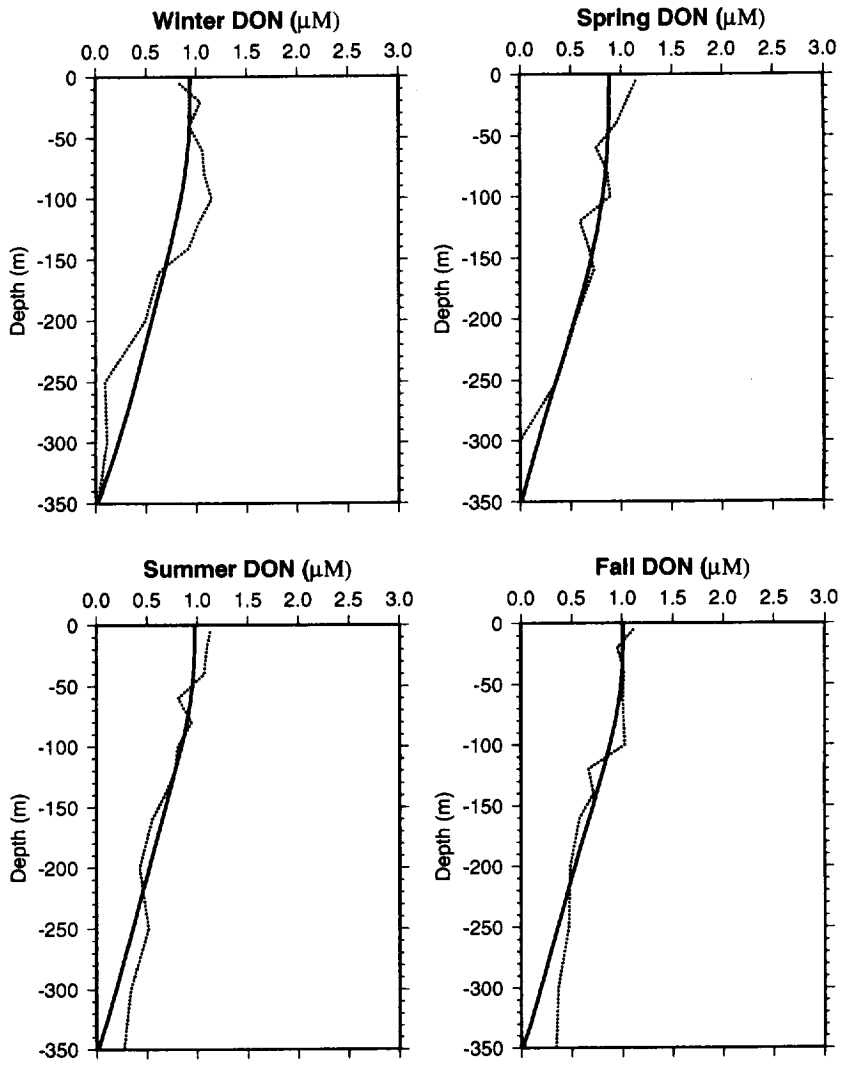

Figure 15: Same as in Figure 9, except for winter, spring, summer, and fall dissolved organic nitrogen (DON). Since there are no direct observations of DON, the DON "observed" seasonal profiles were obtained from the difference between the TON and the PON profiles. Thus no data points are shown, just the averaged profile (dotted line). Labile DON was obtained by subtracting the total DON observed mean value at 350 m.

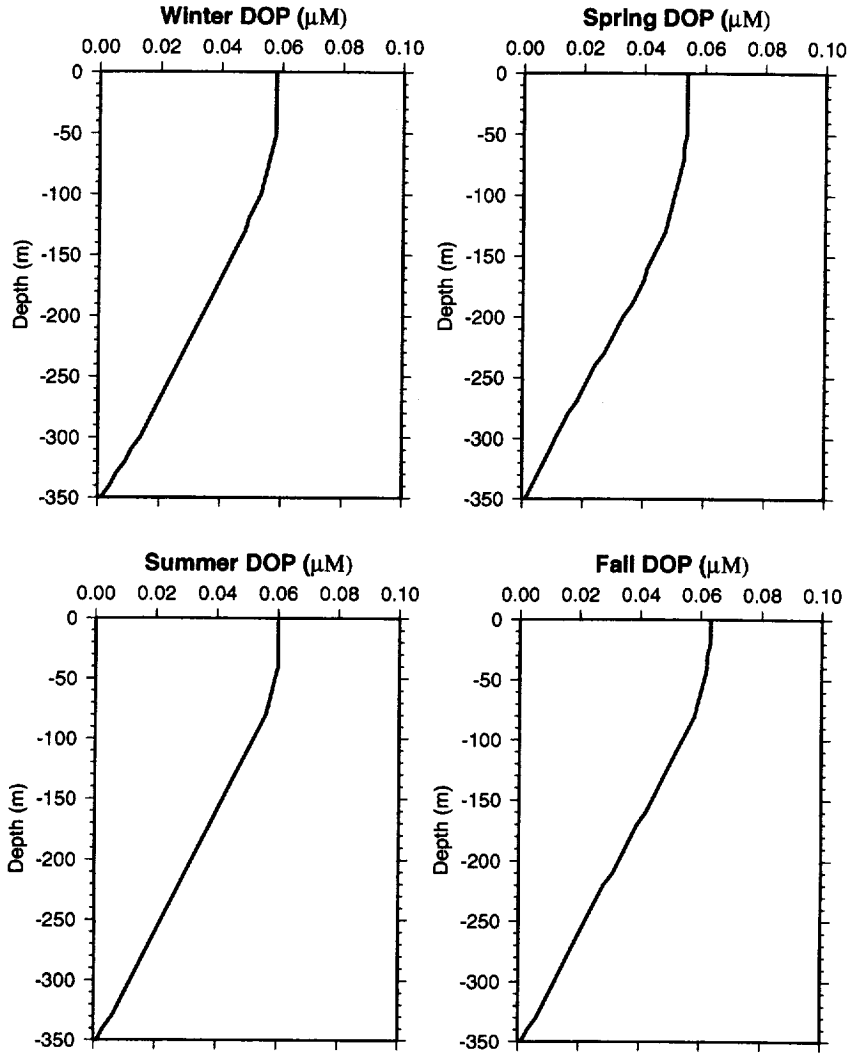

Figure 16: Same as in Figure 15, except for winter, spring, summer, and fall dissolved organic phosphate (DOP). There are no observed values of DOP.

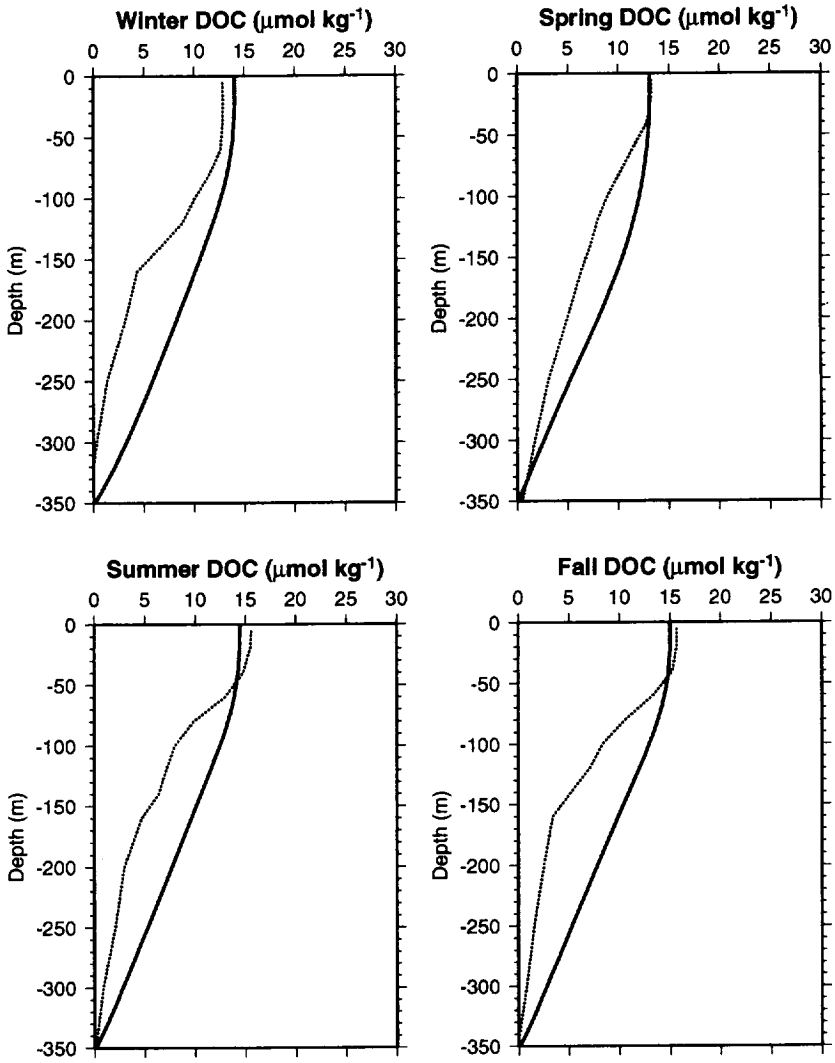

Figure 17: Same as in Figure 15, except for winter, spring, summer, and fall dissolved organic carbon (DOC).

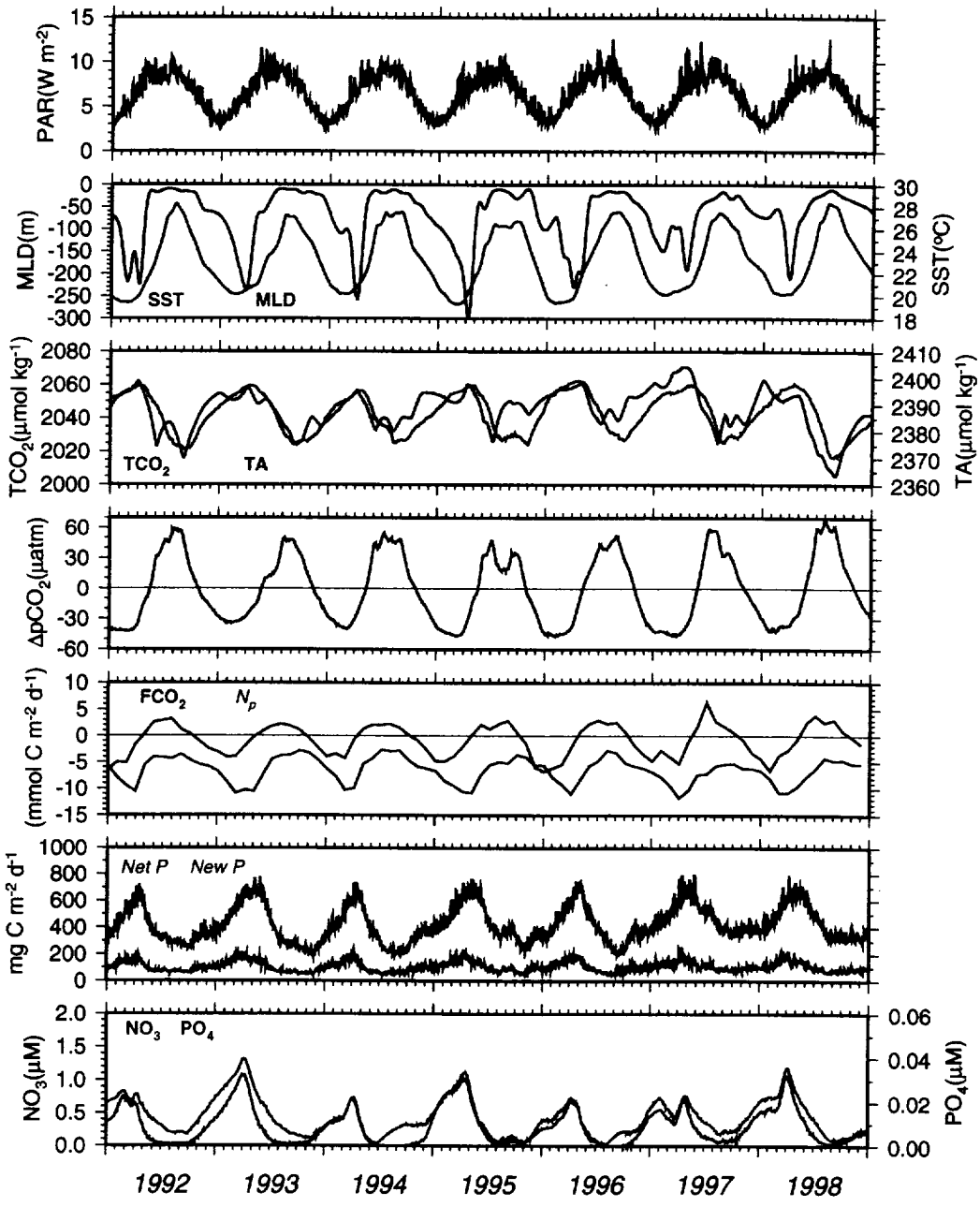

Figure 18: Time series of daily predicted PAR at 50 m, observed mixed layer depth (MLD, green), sea surface temperature (SST, red), surface TCO_2 (blue), surface TA (green), ΔpCO_2, sea-air CO_2 flux (FCO_2, red line), net community production (N_p, blue line), new production ($NewP$, green line), net primary production ($NetP$, blue line) for the whole water column (blue line), and phosphate (PO_4) and nitrate (NO_3) at 50 m.

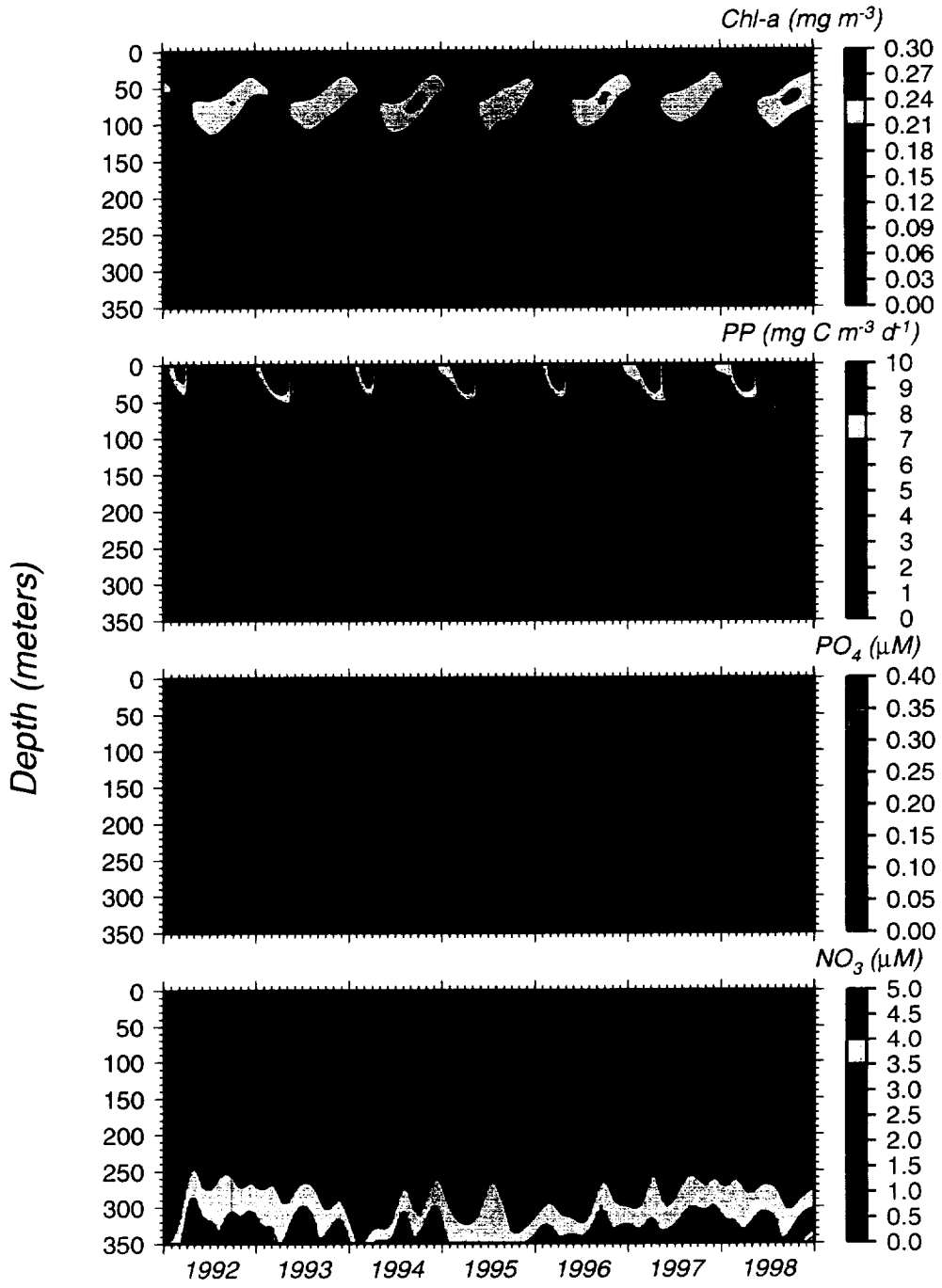

Figure 19: Monthly time series profiles of predicted Chl-*a*, primary production (PP), phosphate (PO_4), and nitrate (NO_3) for 1992-1998.

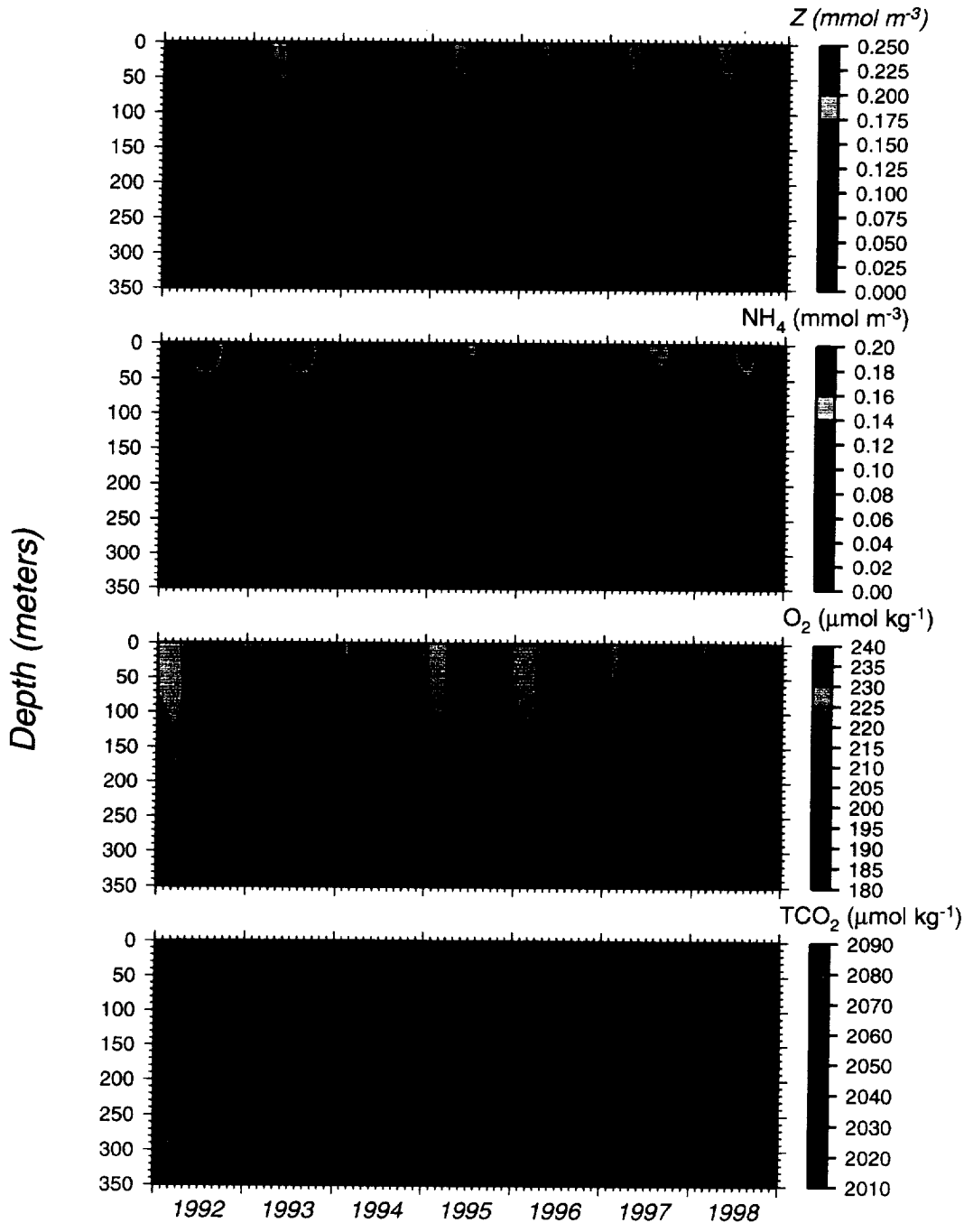

Figure 20: Same as in Figure 19, except for predicted zooplankton (Z), ammonium (NH_4), oxygen (O_2), and total carbon dioxide (TCO_2).

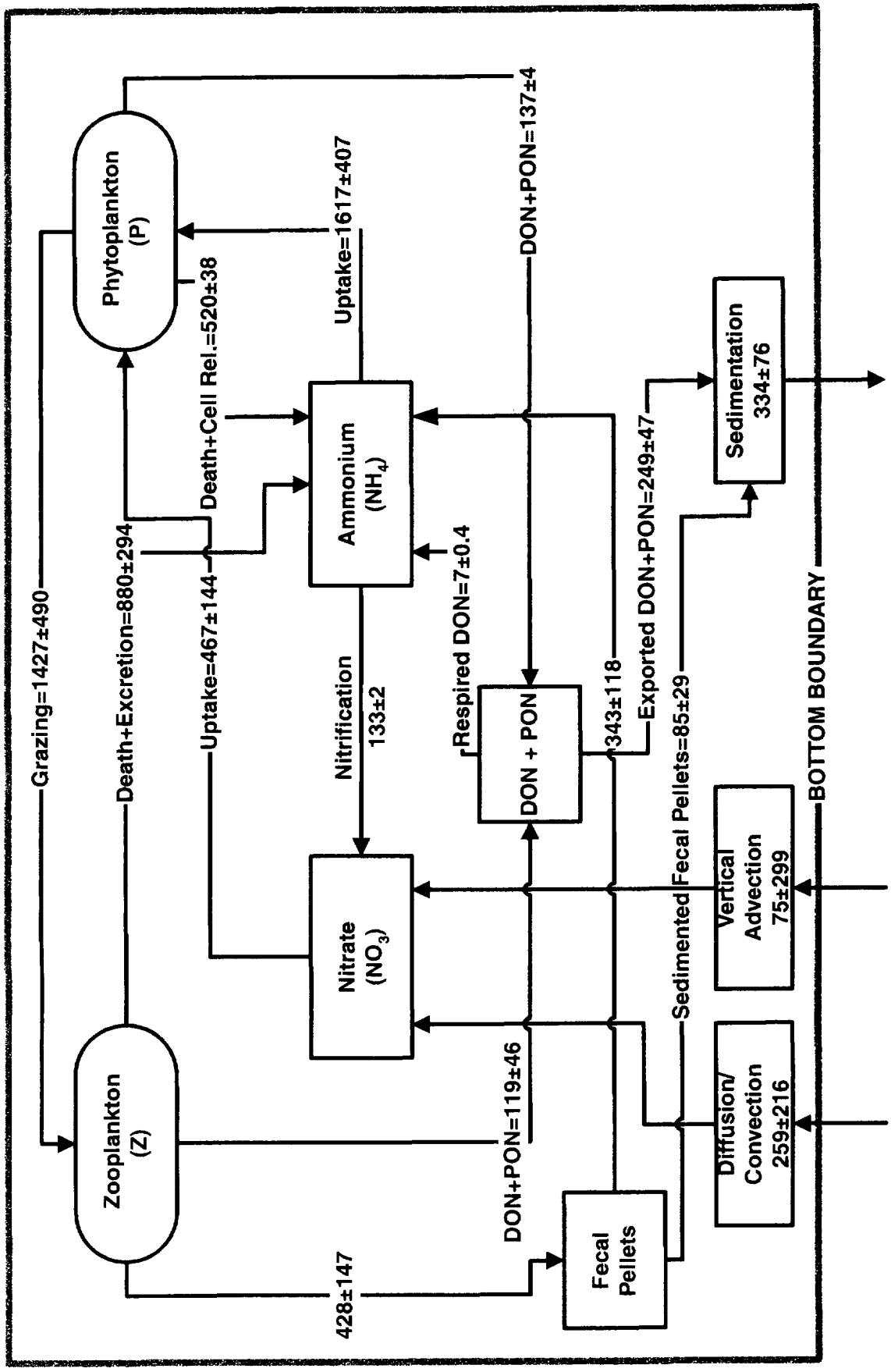

Figure 21: Climatological nitrogen flux (mmol N m^{-2} yr^{-1}) for the BATS study area.

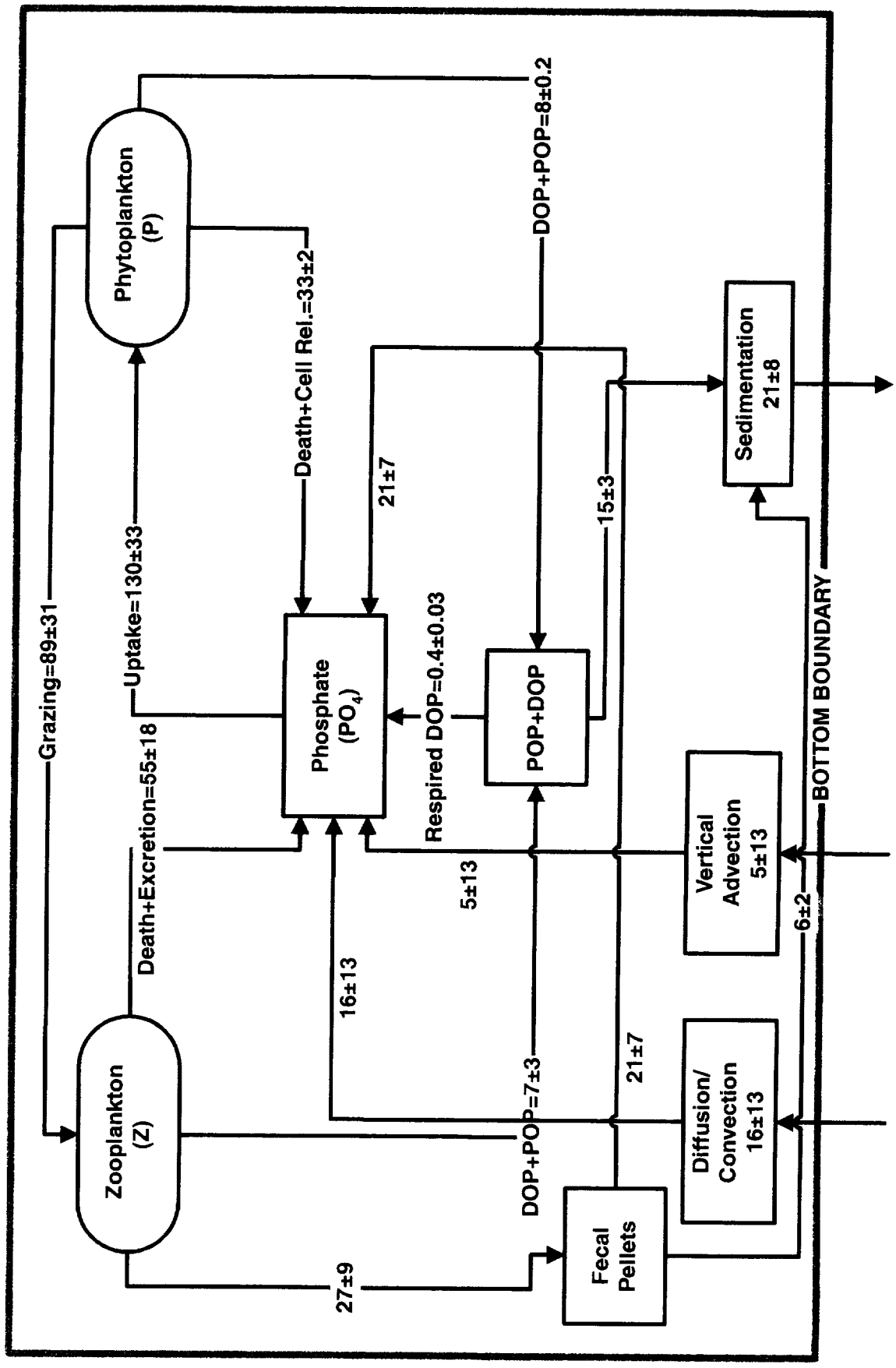

Figure 22: Climatological phosphate flux (mmol P m^{-2} yr^{-1}) for the BATS study area.

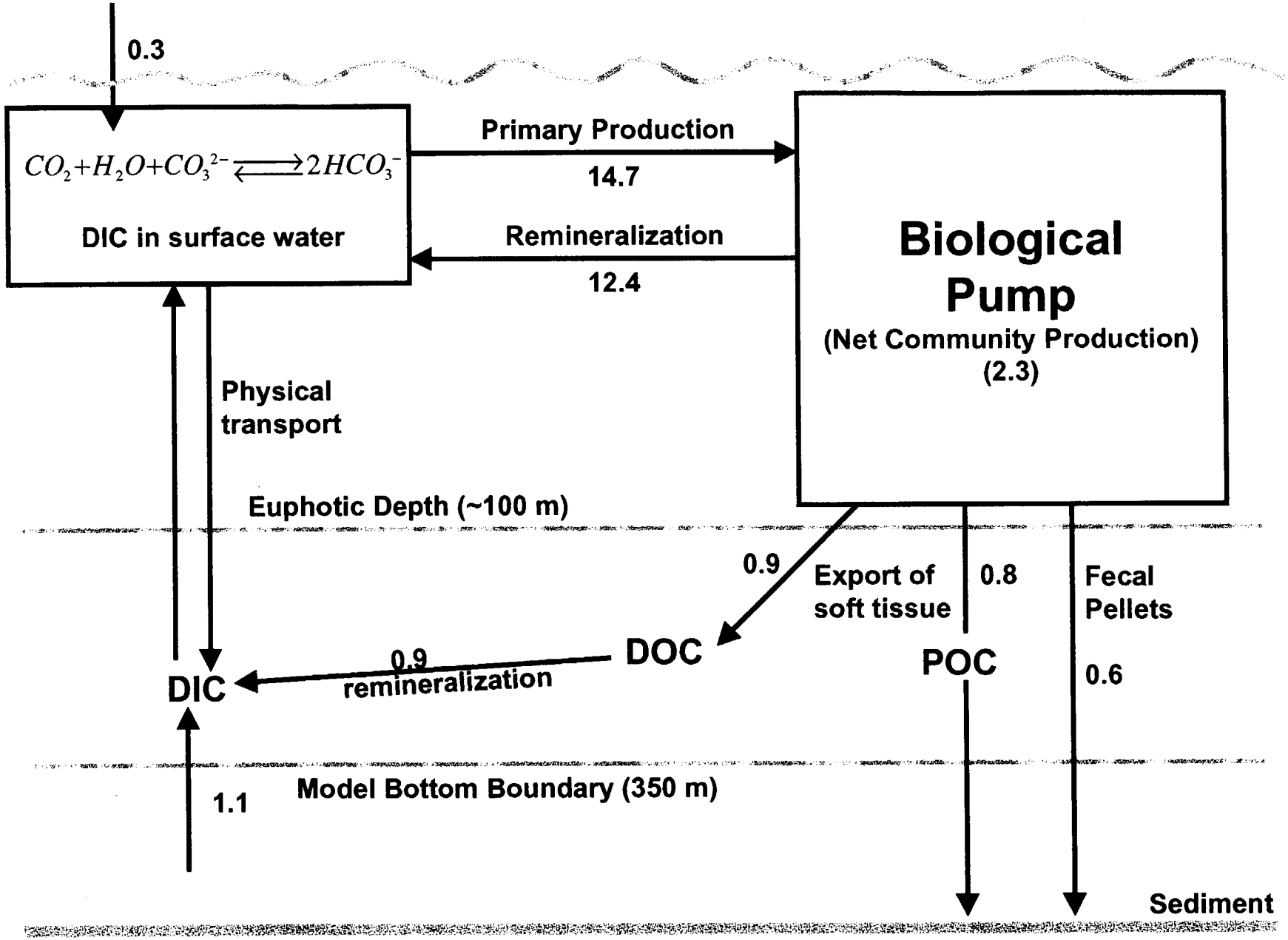

Figure 23: Climatological carbon balance for the BATS study area (1992-1998). Fluxes are in mol C m^{-2} yr^{-1}.

REPORT DOCUMENTATION PAGE

Form Approved
OMB No. 0704-0188

1. AGENCY USE ONLY *(Leave blank)*	2. REPORT DATE	3. REPORT TYPE AND DATES COVERED
	October 2001	TP—2001–209991

4. TITLE AND SUBTITLE
Modeling Biogeochemical-Physical Interactions and Carbon Flux in the Sargasso Sea (Bermuda Atlantic Time-series Study site)

5. FUNDING NUMBERS
970

6. AUTHOR(S)
Sergio R. Signorini, Charles R. McClain, and James R. Christian

7. PERFORMING ORGANIZATION NAME(S) AND ADDRESS (ES)
Goddard Space Flight Center
Greenbelt, Maryland 20771

8. PEFORMING ORGANIZATION REPORT NUMBER
2001-03950-0

9. SPONSORING / MONITORING AGENCY NAME(S) AND ADDRESS (ES)
National Aeronautics and Space Administration
Washington, DC 20546-0001

10. SPONSORING / MONITORING AGENCY REPORT NUMBER
TP—2001–209991

11. SUPPLEMENTARY NOTES
S.R. Signorini: SAIC, Beltsville, Maryland; J.R. Christian: University of Maryland, ESSIC, College Park, Maryland

12a. DISTRIBUTION / AVAILABILITY STATEMENT
Unclassified–Unlimited
Subject Category: 42
Report available from the NASA Center for AeroSpace Information,
7121 Standard Drive, Hanover, MD 21076-1320. (301) 621-0390.

12b. DISTRIBUTION CODE

13. ABSTRACT *(Maximum 200 words)*

An ecosystem-carbon cycle model is used to analyze the biogeochemical-physical interactions and carbon fluxes in the Bermuda Atlantic Time-series Study (BATS) site for the period of 1992-1998. The model results compare well with observations (most variables are within 8% of observed values). The sea-air flux ranges from -0.32 to -0.50 mol C m^{-2} yr^{-1}, depending upon the gas transfer algorithm used. This estimate is within the range (-0.22 to -0.83 mol C m^{-2} yr^{-1}) of previously reported values which indicates that the BATS region is a weak sink of atmospheric CO_2. The overall carbon balance consists of atmospheric CO_2 uptake of 0.3 mol C m^{-2} yr^{-1}, upward dissolved inorganic carbon (DIC) bottom flux of 1.1 mol C m^{-2} yr^{-1}, and carbon export of 1.4 mol C m^{-2} yr^{-1} via sedimentation. Upper ocean DIC levels increased between 1992 and 1996 at a rate of ~1.2 mmol kg^{-1} yr^{-1}, consistent with observations. However, this trend was reversed during 1997-1998 to –2.7 mmol kg^{-1} yr^{-1} in response to hydrographic changes imposed by the El Niño-La Niña transition, which were manifested in the Sargasso Sea by the warmest SST and lowest surface salinity of the period (1992-1998).

14. SUBJECT TERMS	15. NUMBER OF PAGES
Ecosystem-carbon cycle, biogeochemical-physical interactions, carbon fluxes.	37
	16. PRICE CODE

17. SECURITY CLASSIFICATION OF REPORT	18. SECURITY CLASSIFICATION OF THIS PAGE	19. SECURITY CLASSIFICATION OF ABSTRACT	20. LIMITATION OF ABSTRACT
Unclassified	Unclassified	Unclassified	UL